The interplay between molten globule intermediates and heme disassociation characterizes human hemoglobin disassembly

Premila P. Samuel[1,2], Mark A. White[3], William C. Ou[2,4], David A. Case[5], George N. Phillips, Jr.*[2,6], and John S. Olson*[2].

[1]Institute for Quantitative Biomedicine, Rutgers University, Piscataway, NJ 08854; [2]BioSciences Department, Rice University, Houston, TX 77005; [3]Department of Biochemistry and Molecular Biology and The Sealy Center for Structural Biology and Molecular Biophysics, University of Texas Medical Branch, Galveston, TX 77555; [4]University of Texas Southwestern Medical Center, Dallas, TX, 75390; [5]Department of Chemistry & Chemical Biology, Rutgers University, Piscataway, NJ 08854; [6]Department of Chemistry, Rice University, Houston, TX 77005

*Correspondence to:

John S. Olson, olson@rice.edu

George N. Phillips, Jr., georgep@rice.edu

Abstract

Background: Hemoglobin functions as an oxygen transport protein via its hetero-tetrameric structure, with each subunit containing an iron-cofactor heme. We have developed a global disassembly model for human hemoglobin, linking hemin (ferric heme) disassociation and apo (heme-free) subunits unfolding pathways.

Results: Model evaluation was done using circular dichroism and visible absorbance spectroscopy measurements of guanidine hydrochloride-induced holo (heme-bound) hemoglobin disassembly and our previous measurements of apohemoglobin unfolding. The populations of holo intermediates and equilibrium disassembly parameters were determined quantitatively for adult and fetal hemoglobins. Our results show that the key stages for disassembly into unfolded monomers are characterized by hemichrome intermediates with molten globule characteristics. Hemichromes, which occur when both hemin iron axial sites coordinate amino acids, are not energetically favored in native human hemoglobins. However, we have determined that these hexacoordinate iron complexes are important for preventing hemin disassociation from partially unfolded species during early disassembly. Both our model evaluation and independent small angle X-ray scattering measurements demonstrate that heme disassociation during early disassembly leads to loss of the tetrameric structural integrity.

Our model predicts that dimeric and monomeric hemichrome intermediates mediate the disassembly pathway inside red cells where the hemoglobin concentration is very high. This prediction explains why in the red cells of patients with unstable hemoglobinopathies misassembled hemoglobins often get trapped as hemichromes, accumulate into insoluble

Heinz bodies, become deposited at the cell membranes, and often lead to hemolysis. Alternatively, when acellular hemoglobin is diluted into blood plasma after red cell lysis, the disassembly pathway is dominated by early hemin disassociation from the unfolding intermediates. This leads to the generation of higher fractions of apo subunits and free hemin, which is known to damage to the integrity of blood vessel walls.

Conclusions: Our model demonstrates the existence of alternate sets of disassembly/assembly pathways for human hemoglobin, illuminates the pathophysiology of some hemoglobinopathies and other disease states associated with unstable globins and red cell lysis, and provides insights into the factors governing hemoglobin assembly during erythropoiesis.

Keywords: Hemoglobin, protein folding, heme binding, hemoglobinopathies, metalloprotein

Introduction

An interwoven relationship between protein function, structure, and assembly occurs during hemoglobin assembly through step-wise hemin (Fe(II)-protoporphyrin IX) binding that guides the formation of secondary, tertiary, and quaternary protein structures (Figure 1). We depend on erythrocyte-encapsulated hemoglobin (Hb) to transport oxygen in our cardiovascular system [1]. Hb regulates cooperative binding of oxygen to each of its ferrous heme iron atoms via its quaternary conformations. Functional adult HbA consists of α and β globin subunits interacting at both the $\alpha_1\beta_1$ dimer and $\alpha_1\beta_2$ tetramer interfaces. Each globin subunit has 7 or 8 alpha helical segments labeled A to H, and is folded with a heme molecule sandwiched within a cavity between the E and F helices [2, 3].

Building on our earlier work [4], we have been able to establish a global model for human hemoglobin A (HbA) disassembly that involves reversible hemin and subunit disassociations at different disassembly stages (Figure 1). The concept that multiple assembly/disassembly pathways can occur for protein complexes formed by coupling between two protein subunits or between a protein subunit and a cofactor has been explored for other protein systems but not for hemoglobins [5-8]. Our model predicts that the main disassembly pathway for HbA is characterized by both types couplings and will differ markedly between intracellular red cell and acellular blood plasma environments as a result of marked differences in total protein (and heme) concentrations. In order to develop this model, we measured GdnHCl (guanidine hydrochloride) induced disassembly of holoHb at a wide range of protein concentrations. GdnHCl was chosen as a denaturant to avoid irreversible precipitation of hemin [9-11]. We then developed a multilayered analysis approach for Hb disassembly based on our recently published measurements and mechanism for GdnHCl induced unfolding of apoHb [4] and the new holoHb unfolding data generated in this study (Figure 1). Our model was used to analyze simultaneously circular dichroism (CD) measurements of secondary

structure changes in both apo- and holoproteins and populations of hemin-containing unfolding species. The later populations were deconvoluted from visible absorbance measurements at different stages of Hb disassembly. Equilibrium disassembly parameters extrapolated to 0 M GdnHCl concentrations were obtained from fitting of our model describing these changes and populations to the measured data.

Background

Fatal complications in patients with disassembled or misassembled hemoglobins can result from hypoxia, hemolytic anemias, and iron toxicities due to free hemin release into the blood stream [12-19]. The pathogeneses of genetic Hb misassembly and instability diseases often originate from accelerated rates of heme loss, disruption of the inter-subunit interfaces, and accumulation of unstable intermediates states occurring either on- or off-disassembly pathways (Figure 1) [12, 17, 20].

The heme iron is axially coordinated at its proximal side to the Nε2 atom of the F8 histidine on the F helix. In the reduced state, this pentacoordinate iron can bind the key physiological ligands O_2, CO, or NO axially at the sixth coordination position on the distal side of the porphyrin ring [21]. Auto-oxidation of ferrous heme in oxyhemoglobin leads to aqua-metHb, with H_20 bound to Fe(III) protoporphyrin IX (hemin). This metHb form has ≥10,000-fold higher rates of heme disassociation than the corresponding reduced Hb complexes [22-24]. Thus, the first step in disassembly of hemoglobins involves auto-oxidation to the metHb form, which is then followed by protein unfolding and hemin loss. Free heme itself is unstable in the presence of oxygen and auto-oxidizes in milliseconds[21, 25]. Thus, during assembly it is the oxidized form of heme that probably binds to nascent apo polypeptide chains before reduction occurs. In our present study we have focused on the mechanisms and intermediates that occur during aquametHb disassembly.

111 In their disassembly study of sperm whale holo myoglobin (Mb), which is structurally
112 similar to each Hb subunit, Culbertson and Olson [11] developed the strategy of expanding on
113 an apoprotein unfolding scheme to include steps involving hemin dissociation from holoprotein
114 species. Our overall goal was to apply their approach for monomeric Mb to examine
115 quantitatively the effects of hemin binding on the unfolding and disassembly of human holoHb,
116 which is a much more complicated oligomeric system with two types of subunits. We further
117 applied deconvolution methods on visible absorbance spectra to compute the populations of
118 native aquametHb, partially unfolded hemichrome intermediates, and free dissociated hemin in
119 varying mixtures of GdnHCl and holoHb samples. For folded Hbs, hemichromes or
120 hemochromes (ferrous hemichromes) are not native conformers [26]. Ferric hemichromes
121 form via bis-axial coordination of hemin iron to amino acids through combinations of Nε atoms
122 from histidines, S atoms from either methionine or cysteine, and phenoxy O atoms from
123 tyrosine [26].

124 Specific roles and biophysical characteristics of the hemichromes that form during
125 different stages of Hb disassembly have not been well-characterized [27-30]. Our work shows,
126 for the first time, that (a) heterodimeric molten globule hemichromes play both a critical role for
127 $\alpha_1\beta_1$ dimer interface formation and dampening of hemin disassociation during early
128 disassembly stages; and (b) monomeric and dimeric molten globule hemichromes mediate the
129 major pathway for Hb disassembly at high Hb concentrations in erythrocytes. Our prediction of
130 a predominantly hemichrome mediated HbA disassembly pathway in erythrocytes helps to
131 explain why hemoglobinopathies have been often linked to accumulation of denatured
132 hemichrome precipitates that aggregate into inclusion bodies or Heinz bodies (Figure 1A) [12,
133 17, 20].

134 We also observed that a shift between apo- versus holo intermediate mediated Hb
135 disassembly could be modulated by mutations at the inter-subunit interfaces. To test of our

136 disassembly model, we examined fetal holohemoglobin (HbF) because of its intrinsic greater
137 resistance to denaturation relative to HbA [31]. In HbF, γ subunits are expressed in place of
138 the β subunits [1, 32], with amino acid residue differences at the dimer but not tetramer
139 interfaces. The populations of molten hemichrome intermediates during the disassembly of
140 holoHbF are significantly greater than those of holoHbA, and are explained by the increased
141 resistance of the $\alpha_1\gamma_1$ dimer interface to disassociation.
142

143 ## Results

144 **Disassembly mechanism of holoHbA**

145 In our model for Hb disassembly, heterotetrameric holoHb TH_4 initially disassociates
146 into two holoHb dimers (DH_2) without any helical content loss. In addition to undergoing hemin
147 loss leading to the apoHb dimer (D) and its subsequent unfolding (right sides of Figures 1A
148 and 1B), the holodimer (DH_2) can unfold into a dimeric holo molten globule intermediate (IH_2),
149 with a hemichrome absorbance spectrum. Each IH_2 can also further unfold and disassociate
150 into 2 holo monomers (UH). We obtained much better fitting to our spectral measurements
151 when we assigned hemichrome absorbance to the UH species. This assignment is supported
152 by previous experimental studies, which showed that isolated aquamet α and β monomers
153 form unstable hemichromes [29, 33]. Hemin disassociation from UH leads to formation of the
154 apo monomer U states, with residual helical content, and then the completely unfolded chains
155 at very high denaturant concentrations.

156 Complete chemical extraction of hemin from folded Hbs leads to a heterodimeric apoHb
157 (D) that has undergone 30% helical content loss[4, 34]. Our previous studies show that this D
158 state initially unfolds into a molten globule apo dimer (I), which has lost 70% of its original α-
159 helical content relative to holoHbA. Next, this molten globule apo I state disassociates into
160 unfolded monomers (U) with only residual helical content (≤ 10 %). These monomers then can

161 either interact non-specifically to form transient dimers (U_2), or completely unfold into
162 polypeptide chains (U_C) [4]. The TH_4 disassembly scheme in this present study expands the
163 apoHb model (Figure 1B, right side, gray section) described above to include the binding of
164 hemin (H) to the various D, I, and U states and the formation of hemin containing tetramers
165 (TH_4 and TH_2 states in Figure 1). We did not include the formation of tetrameric
166 apohemoglobins in our models because past studies have shown that native human apoHbs
167 can only exist as dimers, and not as tetramers [4, 35-37]. The accompanying loss of α-helical
168 content in apoHb due to hemin dissociation is predicted to be occurring around the heme
169 cavity region which also forms the tetramer ($\alpha_1\beta_2$) interface and thereby causing the tetramer
170 disassembly into dimers [4, 34].

171 Previous studies have shown that native metHbA undergoes non-cooperative hemin
172 disassociation with β subunits having a faster hemin loss rate and presumably lower hemin
173 affinity [22, 38-40]. Therefore, we also incorporated non-cooperative hemin binding into our
174 model (Figure 1) by taking into account sequential hemin disassociation from the DH_2 and IH_2
175 states. However, we made no assumptions about the relative hemin affinities of the two
176 different types of subunits and instead assigned equilibrium constants for each sequential
177 dissociation step. In our model fitting, differences between the subunits would be manifested in
178 the extent of the differences between the first and second hemin dissociation or association
179 equilibrium constants.

180 Thus in our model hemin (H) disassociates first from one subunit in DH_2, resulting in the
181 dimeric semi-holoHb (DH) formation, and then hemin disassociation from DH leads to the
182 apoHb D state. Similarly for IH_2, hemin disassociation occur first from one subunit leading to
183 initial formation of semi-hemichrome (IH) and then the next dissociation leads to the formation
184 of apo molten globule (I). Past studies have suggested the semi-holohemoglobin formation

185 occurs by either hemin disassociation from the β subunits in holo tetramers/holo dimers or
186 alternatively by hemin binding to the α subunits first in the apoHbs [39, 41].

187 Given the weak affinity of hemin for unfolded proteins [9, 11, 42, 43], the lack of
188 structural evidence about unfolded states, and the limitations of spectroscopic measurements,
189 we assumed no differences in hemin affinity between α versus β variants of U monomers
190 ($K_{U,UH}$) (Figure 1). Non-specific hemin binding to the U_2 and U_C could not be accurately defined
191 because only free hemin visible absorbance spectra could be observed after the loss of all
192 helical content in the unfolded monomers.

193 All of these reversible disassembly stages described in this section were incorporated
194 into our overall scheme and are represented by Model 1 (blue arrows) in Figure 1. We also
195 considered an additional step involving semi-holo tetramer formation, which was incorporated
196 into Model 2 (both blue and black arrows). In this second model, TH_4 undergoes disassociation
197 of two hemin molecules initially from the subunit type with lower hemin affinity to form the
198 tetrameric semi- holoHb (TH_2).

199

200 **Spectroscopic measurements of holoHb disassembly**

201 GdnHCl-induced disassembly of holo- aquametHbA (Figures 2 and 3) and HbF (Figure
202 4) was examined as function of total protein concentration by measuring simultaneously both
203 heme visible absorbance and protein CD spectral changes. With increasing denaturant
204 concentration, holoHb unfolds and undergoes both hemin disassociation (Figures 2, 3C, and
205 4C) and loss of α-helical content (Figures 3D and 4D). CD signal changes at 222 nm were
206 used as a measure of the fraction of α-helical content present in the protein relative to that of
207 folded holoHb (Figures 3D and 4D [4]). The changes in hemin absorbance spectra were used
208 to compute populations of the various holo species during disassembly and free hemin (H).

209 As holoHb disassembles with increasing GdnHCl concentration, we observed dramatic
210 shifts in the heme visible absorbance spectra as shown in Figure 2A. Initially, at low [GdnHCl],
211 the observed visible absorbance spectra were characterized by features that are unique to
212 high-spin aquametHb (Figure 2B), including a sharp, dominant Soret absorbance peak at 405
213 nm and additional smaller peaks at 500 nm and 630 nm. At high [GdnHCl] corresponding to
214 when only residual (≤ 10%) or no alpha-helical content remains in the protein (Figures 2A and
215 3D), the absorbance spectra were characterized by features that were unique for high-spin
216 free hemin in free solution, including a broad Soret absorbance peak around 370 nm and
217 additional smaller peaks around 510 nm and 630 nm (Figure 2B) [11, 21, 44-46]. During
218 intermediate stages of Hb disassembly, another distinct absorbance spectrum appears for both
219 HbA and HbF and is indicative of a low-spin hemichrome (Figures 2, 3C, and 4C).
220 Hemichrome absorbance spectra are characterized by a distinct and narrow red-shifted Soret
221 absorbance peak around 413 nm and Q bands or visible region peaks at 535 nm and 565 nm
222 (Figure 2B)[11, 26, 47, 48].
223 As described in Methods, we deconvoluted the heterogeneous visible absorbance
224 spectral curves obtained for GdnHCl induced Hb disassembly using the three component
225 spectra for native aquamet, hemichrome intermediates, and free hemin shown in Figure 2B.
226 The differing population fractions of these species were computed as the GdnHCl titrations
227 proceeded, and the results for aquametHbA are shown in Panels 3A, 3B, and 3C and for
228 aquametHbF in Panels 4A, 4B, and 4C. The hemichrome population reaches a maxima at the
229 beginning of the 2nd phase of unfolding, corresponding to when the protein has lost ~60 % of
230 its alpha-helical content and forms a molten globule (Figures 2A, 3B, 3D, 4B, and 4D).
231
232
233

234 **Hemichrome mediated resistance to hemin disassociation and subunit interface**
235 **disassembly**

236 As shown for HbA in Figure 3D, the CD curves shifted towards higher [GdnHCl] in the
237 presence of bound hemin in both HbA and HbF (see also [4]). This shift is indicative of the
238 higher stability of holoHb relative to apoHb [4]. Previously, we had determined that during
239 apoHb unfolding, the 1st phase likely involves the unfolding of the heme pocket while the 2nd
240 phase corresponds to the disassembly of the heterodimeric molten globule [4]. For apoHbs,
241 the protein concentration dependency of the 2nd phase of unfolding demonstrated the
242 disassociation of the $\alpha_1\beta_1$ and $\alpha_1\gamma_1$ dimeric molten globules into unfolded monomers [4]. The
243 same interpretation applies for the unfolding curves of holo- HbA and HbF in this study. Again,
244 increasing protein concentration shifts the second phase for loss of α-helical content to higher
245 [GdnHCl] (Figures 3D and 4D). Similarly, the loss of hemichrome populations (Figures 3B and
246 4B) and the appearance of free hemin (Figures 3C and 4C) are shifted towards higher
247 [GdnHCl], demonstrating that there is greater resistance to hemin disassociation with
248 increasing protein concentration. These CD and visible absorbance analyses together
249 demonstrate that the bound hemin in the hemichrome state strengthens the α1β1 and the α1γ1
250 interfaces in the molten globules.

251 In our previous studies on apoHb unfolding, we determined that the $\alpha_1\gamma_1$ dimer interface
252 in HbF is more resistant to disassembly relative to HbA, with a monomer to dimer association
253 constant (K_{UI}) of 8.4×10^9 M^{-1} whereas the $\alpha_1\beta_1$ interface in HbA has about a 10-fold lower K_{UI} at
254 6.6×10^8 M^{-1} [4] (Table 1). Correspondingly, the HbF hemichrome population showed a higher
255 resistance to hemin disassociation during the 2nd phase of unfolding (Figures 5B and
256 Supplement 1B). Similarly, rHb0.1, a recombinant variant of HbA with a genetic cross-linker
257 between the α subunits, is also observed to have a larger hemichrome population at high
258 [GdnHCl] than both HbA and HbF (Figures 5B and Supplement 1B). The covalently

259 crosslinked aporHb0.1 tetramer has been previously shown to be more resistant to
260 disassembly during the second phase than either HbA or HbF apo dimers because two $\alpha 1\beta 1$
261 interfaces have to be disrupted in rHb0.1 to generate 2 unfolded β monomers and a di-α
262 subunit [4].
263

264 **Table 1. Fitted equilibrium disassembly parameters for HbA and HbF**

	HbA	HbF
$K_{2,4}$ (M^{-1})	1.0×10^{5}	1.0×10^{5}
$K_{DH,DH2}$ (M^{-1})	1.3×10^{10}	1.3×10^{11}
$K_{D,DH}$ (M^{-1})	1.3×10^{11}	2.5×10^{11}
$K_{IH,IH2}$ (M^{-1})	3.3×10^{8}	1.4×10^{9}
$K_{I,IH}$ (M^{-1})	1.1×10^{11}	7.8×10^{11}
$K_{U,UH}$ (M^{-1})	2.9×10^{7}	8.4×10^{7}
$m_{2,4}$ (kJ mol^{-1} M^{-1})	20.0	20.0
$m_{DH,DH2}$ (kJ mol^{-1} M^{-1})	10.3	9.9
$m_{D,DH}$ (kJ mol^{-1} M^{-1})	10.3	9.9
$m_{IH,IH2}$ (kJ mol^{-1} M^{-1})	10.3	10.7
$m_{I,IH}$ (kJ mol^{-1} M^{-1})	10.3	10.7
$m_{U,UH}$ (kJ mol^{-1} M^{-1})	5.1	5.2
S_{TH4}	1.00	1.00
S_{DH2}	1.00	1.00
S_{DH}	0.87	0.87
S_{IH2}	0.43	0.59
S_{IH}	0.42	0.34
S_{UH}	0.20	0.30
$K_{I,D}$ [a]	164	128
$K_{U,I}$ [a] (M^{-1})	6.6×10^{8}	8.4×10^{9}
$K_{U2,U}$ [a] (M)	5.6×10^{-7}	1.7×10^{-8}
$K_{UC,U}$ [a]	1190	921
$m_{I,D}$ [a] (kJ mol^{-1} M^{-1})	16.2	17.5
$m_{U,I}$ [a] (kJ mol^{-1} M^{-1})	11.6	12.7
$m_{U2,U}$ [a] (kJ mol^{-1} M^{-1})	-3.9	-6.8
$m_{UC,U}$ [a] (kJ mol^{-1} M^{-1})	5.4	5.4
S_D [a]	0.70	0.73
S_I [a]	0.30	0.33
S_U [a]	0.062	0.08
S_{U2} [a]	0.015	0.02
S_{UC} [a]	0.0034	0.006

265 The disassembly parameters as a factor of hemin were fitted according to model 1.
266 [a]Parameters for the apoHb part of the disassembly had been determined in our previously
267 published work[4]
268

269 For both HbA and HbF, protein concentration dependency was not observed during the
270 1st phase of unfolding either in the CD curves or the population fractions of the heme spectral
271 species (Figures 3C, 3D, 4C, and 4D). Hemichromes start to appear during the 1st phase and,
272 in fact, seem to be playing a key role in reducing hemin loss during the early disassembly
273 stages for both HbA and HbF (i.e. little free hemin is present until [GdnHCl] ≥ 1.5 to 2 M). If
274 significant hemin disassociation had been occurring from folded metHb or the newly formed
275 hemichromes, we should have observed population shifts in the curves for native aquametHb
276 and changes in the first phase for the appearance of free hemin as protein concentration
277 increased (Figures 3A,C and 4A,C). Instead, conformational changes around the heme pocket
278 region during the 1st phase promoted a high-spin metHb to low-spin hemichrome transition with
279 heme still bound in the protein. This conformation change is likely induced by the loss of α-
280 helicity around the heme pocket region similar to what occurs during the 1st phase of apoHb
281 unfolding [4].

282 We initially expected to see a dependence on protein concentration for the initial phase
283 of the CD change due to holo tetramer to holo dimer dissociation. However, none was
284 observed due to the large tetramer to dimer dissociation constant of aquametHb, which is ~10
285 μM [49]. The threshold of the CD photomultiplier limited the range of holoprotein
286 concentrations to be examined. Within the smaller range that we could examine (1 to ~60 μM
287 total heme), our modeling (Figure 1) predicted that the tetramer to dimer disassembly was
288 occurring at very low denaturant concentrations before any significant heme pocket unfolding
289 or hemin dissociation occurred. However, if we could have carried out experiments in the
290 millimolar hemoglobin concentration region, our model does predict that we would observe
291 protein concentration effects during the first phases of disassembly (see the results section,
292 "*Modeling HbA disassembly in erythrocytes and in blood plasma*").

293 The E7 histidine is the nearest amino acid that can coordinate with the hemin iron at the
294 distal side of the porphyrin ring in Hb. His-E7 often stabilizes exogenous ligands bound to
295 heme iron through hydrogen bonding with the Nε2 atom. However, the Nε2 atom is still at a
296 non-bonding distance of ~4.1 Å from the hemin iron in native metHbA, and a water molecule is
297 coordinated instead (see PDB 3P5Q [50] and [26]). Although we assume the major
298 hemichrome species during native HbA disassembly is most likely due to hemin iron
299 hexacoordination to both the F8 and E7 histidines, to the best of our knowledge, no direct
300 structural evidence for this assumption exists.

301 Different pathways for hemichrome formation are almost certainly occurring because
302 hemichrome spectra are still observed for the recombinant metHb α(H58L/V62F)β(H63L/V67F)
303 quadruple mutant, in which both distal histidines were replaced with leucines (Figure 5B).
304 However, the population fraction of the hemichrome intermediate formed during disassembly
305 of the mutant is roughly half that observed for native HbA, implying less stable
306 hexacoordination (Figure 5B). In our recent apoHb unfolding studies, the mutant apoHb
307 showed increased resistance to unfolding during the 1st phase due to the introduction of the
308 large and apolar residues in the heme cavity[4]. However, the mutant also showed increased
309 hemin disassociation during the 1st phase of disassembly (Figures 5A and Supplement 1B).
310 Past studies of His-E7 to Leu mutations in both Hbs and Mbs attributed the marked increases
311 observed in rates of hemin dissociation to loss of hydrogen bonding between the E7 side chain
312 and the coordinated H_20 molecule [51, 52]. Our disassembly results now suggest that the role
313 of hemichrome formation should also be considered when determining the rates of net hemin
314 dissociation since these species are clearly intermediates in holoHb unfolding.
315

316 **Deriving disassembly parameters**

317 The assembly constants defined in Figure 1B and listed in Table 1 were obtained by
318 extrapolation to 0 M GdnHCl concentration or x, and are represented by the K^0 values in eqs 1
319 and 2. This extrapolation was done using the dependence of the K constants on [GdnHCl] or x
320 as shown in eqs 1 and 2. The apoHb folding constants in Table 1 and eq 2 were originally
321 derived in our earlier work [4]. The m values describe the dependence of the assembly free
322 energies on [GdnHCl] and absolute temperature (T). The K parameters containing H
323 subscripts in eq 1 define hemin or H binding to the various apoglobin intermediates in Figure
324 1B, and $K_{2,4}$ defines the holo metHb dimer to tetramer association equilibrium constant.

325

$$K_{2,4} = \frac{[TH_4]}{[DH_2]^2} = K^0_{2,4} \exp\left(\frac{-m_{2,4}x}{RT}\right)$$

$$K_{DH,DH2} = \frac{[DH_2]}{[DH][H]} = K^0_{DH,DH2} \exp\left(\frac{-m_{DH,DH2}x}{RT}\right)$$

$$K_{D,DH} = \frac{[DH]}{[D][H]} = K^0_{D,DH} \exp\left(\frac{-m_{D,DH}x}{RT}\right)$$

326 $$K_{IH,IH2} = \frac{[IH_2]}{[IH][H]} = K^0_{IH,IH2} \exp\left(\frac{-m_{IH,IH2}x}{RT}\right) \qquad (1)$$

$$K_{I,IH} = \frac{[IH]}{[I][H]} = K^0_{I,IH} \exp\left(\frac{-m_{I,IH}x}{RT}\right)$$

$$K_{U,UH} = \frac{[UH]}{[U][H]} = K^0_{I,IH} \exp\left(\frac{-m_{U,UH}x}{RT}\right)$$

$$K_{TH4,TH2} = \frac{[TH_2][H]^2}{TH_4} = (K^0_{TH4,TH2}) \exp\left(\frac{m_{TH4,TH2}x}{RT}\right)$$

327

For our overall Hb disassembly/assembly scheme described in model 1 (Figure 1), the theoretical values of total protein concentration [P] on per subunit basis and total free hemin concentration [Free hemin] in solution were computed from the concentrations of the various species in eqs 3 and 4, respectively. This theoretical [P] value should equate to y, the experimentally determined per subunit Hb concentration. Because there is no excess hemin in the original solutions, [free hemin] in eq 4 will equate to [H] in eq 1. [Free hemin] in eq 4 is computed from the sum of the concentrations of the apo subunits in all the apo- and semi-holo species. For the alternative model 2 that included semi-holo tetramers, [P] and [free hemin] were re-derived with the addition of the terms $4[TH_2]$ and $2[TH_2]$ to the right sides of eqs 3 and 4 respectively.

$$K_{I,D} = \frac{[D]}{[I]} = K^0_{I,D} \exp\left(\frac{-m_{I,D}x}{RT}\right)$$

$$K_{U,I} = \frac{[I]}{[U]^2} = K^0_{U,I} \exp\left(\frac{-m_{U,I}x}{RT}\right)$$

$$K_{UC,U} = \frac{[U]}{[U_C]} = K^0_{UC,U} \exp\left(\frac{-m_{UC,U}x}{RT}\right) \qquad (2)$$

$$K_{U2,U} = \frac{[U]^2}{[U2]} = K^0_{U2,U} \exp\left(\frac{-m_{U2,U}x}{RT}\right)$$

$$[P] = 4[TH_4] + 2[DH_2] + 2[DH] + 2[IH_2] + 2[IH] + [UH] + 2[D] + 2[I] + [U] + [U_C] + 2[U_2] \qquad (3)$$

$$[\text{Free hemin}] = [DH] + [IH] + 2[D] + 2[I] + [U] + [U_C] + 2[U_2] \qquad (4)$$

The general population fraction Y_i on per subunit basis for a specific folding species (i) is described in eq 5. In eq 5, specific examples are also given for the free hemin fraction (Y_H)

346 and holoHb tetramer population fraction (Y_{TH4}) from model 1. The total population fraction of
347 folded holoHbs, encompassing both the holoHb dimers and tetramers, is defined as Y_{Folded}
348 $_{holoHb} = Y_{TH4} + Y_{DH2} + 0.5Y_{DH}$ for model 1, and $Y_{Folded\ holoHb} = Y_{TH4} + Y_{DH2} + 0.5(Y_{TH2} + Y_{DH2})$ for
349 model 2. In both models, the total population fraction of hemichromes was evaluated as
350 $Y_{Hemichromes} = Y_{IH2} + 0.5Y_{IH} + Y_{UH}$.

351 The theoretical $Y_{Folded\ holoHb}$ value was assumed to correspond to the population fraction
352 of native metHb spectral species (red spectrum in Figure 2B) derived experimentally from the
353 deconvolution of the measured visible spectra as a function of [GdnHCl]. $Y_{Hemichrome}$ and Y_H
354 were assumed to correspond respectively to the fractions of the low spin hemichrome
355 spectrum (blue spectrum in Figure 2B) and high spin free hemin spectrum (green spectrum in
356 Figure 2B) in our measured visible absorbance data. A weight of 0.5 was assigned to the semi-
357 holoHb Y values in the expressions of $Y_{Hemichrome}$ and $Y_{Folded\ holoHb}$ to account for the subunits
358 present that already had undergone hemin disassociation. The theoretical normalized total CD
359 signal, S_{Total}, is a measure of fractional alpha-helicity of protein at 222 nm relative to folded
360 holoHb. S_{Total} was defined as the sum of the product of Y_i and intrinsic normalized CD signal S_i
361 for each folding species (not including H) as shown in eq 6. S_i is independent of x and y and is
362 defined as the fraction of α-helical content of species i relative to folded holoHb.

363

$$Y_i = \frac{<\text{Number of subunits per i}> [i]}{P}$$

e.g. for Model 1

364 $$Y_H = \frac{[H]}{4[TH_4] + 2[DH_2] + 2[DH] + 2[IH_2] + 2[IH] + [UH] + 2[D] + 2[I] + [U] + [UC] + 2[U_2]} \quad (5)$$

$$Y_{TH4} = \frac{4[TH_4]}{4[TH_4] + 2[DH_2] + 2[DH] + 2[IH_2] + 2[IH] + [UH] + 2[D] + 2[I] + [U] + [UC] + 2[U_2]}$$

365

366

367
$$S_{Total} = \sum S_i Y_i$$
e.g. for Model 1,
$$S_{Total} = S_{TH4}Y_{TH4} + S_{DH2}Y_{DH2} + S_{DH}Y_{DH} + S_{IH2}Y_{IH2} + S_{IH}Y_{IH} + S_{UH}Y_{UH} \ldots + S_D Y_D + S_I Y_I + S_U Y_U + S_{UC}Y_{UC} + S_{U2}Y_{U2} \quad (6)$$

368

369 The K, m, and S_i values characterizing holoHb unfolding were estimated by global fitting
370 of (a) specific Y_i or sum of Y_i values to corresponding native metHb, hemichrome, and free
371 hemin populations obtained from deconvolution of the visible spectral data; and (b) S_{Total} to the
372 experimental CD values that were normalized against the α-helical content of folded holoHb
373 (Figures 3, 4, and Table 1). The fits to these experimental measurements were done as a
374 function of x (GdnHCl concentration) and y (total protein concentration) variables for both
375 holoHbA and holoHbF. The K, m, and Si values for the apoHb unfolding steps were fixed to the
376 values determined from our previous, independent apoHb unfolding studies [4, 11]. The m
377 values for the association constants for hemin binding to the folded heme pockets were set
378 equal to each other (e.g. $m_{DH,DH2} = m_{D,DH}$) and the m values for the parameters describing
379 hemin binding to the molten dimers were also set equal to each other (e.g. $m_{IH,IH2} = m_{I,IH}$)
380 (Table 1, Supplement Table 1).

381 The $K_{2,4}$ value for metHb dimer-dimer association was initially set to $1x10^5$ M^{-1} for
382 metHbA based on previous studies, and since there is no protein sequence difference at the
383 tetramer interface between HbA and HbF, the same value was used for HbF [49]. This number
384 did not change much during the model fittings. The lack of change was likely due to: (a) the
385 absolute value of $K_{2,4}$ being poorly defined but in the $1x10^5$ M^{-1} range; and (b) the tetramer
386 dissociation being complete at very low denaturant concentrations ([GdnHCl] ≤ 0.5 M).

387 The Y_i values had to be computed first by defining them in terms of the K constants at
388 different x and y values (left sides of eqs 1 and 2) for comparison with the experimental data.

For this purpose, [U] and [H] values at a given x and y were obtained by numerically applying Newton's method [53] for systems of non-linear equations (eqs 7-8) expanded from the definitions of [P] (e.g. eq 3) and [Free hemin] (e.g. eq 4). As shown for Model 1 in eqs 7-8, all species were expanded only in terms of [U], [H], and K values. These initial values of [U] and [H] were used to compute new values of Y_i.

Starting from these initial estimates of Y_i, lsqcurvefit function (a non-linear least-squares solver) in MATLAB R2017a (The MathWorks, Inc., Natick, MA) was applied to globally fit the theoretical models to the experimental measurements as shown in Figures 3, 4, and S2. An algorithm was written in MATLAB R2017a (The MathWorks, Inc., Natick, MA) to apply the numerical analysis method and fitting function in an iterative loop where the K, m, and S_i parameters updated from each optimization loop was fed back to the numerical analysis part of the algorithm to obtain a new sets of [U] and [H] values. The implementation of the loop is stopped when the best fit between the experiment and model is reached as defined by a minimum steady state value of χ2, the squared residual difference between the models and experimental measurements.

$$
\begin{aligned}
&[P] - y = 0 \\
&\text{For Model 1,} \\
&4[TH_4] + 2[DH_2] + 2[IH_2] + 2[DH] + 2[IH] + [UH] + 2[D] + 2[I] + [U] + [U_C] + 2[U_2] - y = 0 \\
&4K_{TH4}(K_{DH,DH2}K_{D,DH}K_{I,D}K_{U,I})^2[U]^4[H]^4 + 2K_{DH,DH2}K_{D,DH}K_{I,D}K_{U,I}[U]^2[H]^2 + \ldots \\
&2K_{IH,IH2}K_{I,IH}K_{U,I}[U]^2[H]^2 + 2K_{D,DH}K_{I,D}K_{U,I}[U]^2[H] + 2K_{I,IH}K_{U,I}[U]^2[H] + \ldots \\
&K_{U,UH}[U][H] + 2K_{I,D}K_{U,I}[U]^2 + 2K_{U,I}[U]^2 + [U] + \frac{[U]}{K_{UC,U}} + 2\frac{[U]^2}{K_{U2,U}} - y = 0
\end{aligned}
\tag{7}
$$

407 [Free hemin] - [H] = 0

For Model 1,

$$[DH]+[IH]+2[D]+2[I]+[U]+[U_C]+2[U_2]-[H]=0 \quad (8)$$

$$K_{D,DH}K_{I,D}K_{U,I}[U]^2[H]+K_{I,IH}K_{U,I}[U]^2[H]+...$$

$$2K_{I,D}K_{U,I}[U]^2+2K_{U,I}[U]^2+[U]+\frac{[U]}{K_{UC,U}}+2\frac{[U]^2}{K_{U2,U}}-[H]=0$$

408

409 Our overall disassembly Model 1 (Figure 1, blue arrows) was fitted to HbA unfolding data
410 (Figure 3) using the optimized parameters in Table 1. A χ2 value of 0.76 was obtained.

411 The alternative Model 2 was proposed in order to try to determine the hemin binding
412 constant for the low affinity subunit (probably β) in tetrameric HbA (Figure 1). When HbA
413 unfolding data were fitted to the model 2 (Figure Supplement 2) with 2 additional degrees of
414 freedom (Table Supplement 2), there were only small changes in the goodness of the fit
415 (χ2=0.65). More importantly, the population fraction of semi-holo tetramers, with disassociated
416 hemin from β subunits, was always close to 0 (Figure Supplement 2A inset). Even this more
417 complex scheme indicated that small amounts of GdnHCl were sufficient to disrupt the weak
418 holo tetramer interface before any significant unfolding or hemin dissociation occurs at the
419 protein concentrations that were accessible to our spectral measurements (dashed lines in
420 Figures 3A and Supplement 2A).

421 When when Model 2 was simulated later at high protein concentrations (~mM range)
422 (see next section and Figure Supplement 3A), the population of semi-holotetramers was still
423 almost 0. This result also suggests that semi-holo tetramers are not a predominant species
424 during HbA assembly, and heme insertion is occurring much earlier during dimer assembly
425 (see Discussion). Furthermore, other kinetic studies have documented that hemin loss rates
426 increase dramatically when Hb tetramers dissociate into dimers [22, 24, 54]. Thus, we chose to
427 consider only the simpler Model 1, in which complete dissociation of holo tetramers into dimers
428 occurs during HbA disassembly before either hemin loss or unfolding.

429 This model (Figure 1) predicts sequential binding of hemin to the apo dimer with
430 association equilibrium constants equal to $K_{D,DH}$ = 1.3 X 10^{11} M^{-1} for the first step and $K_{DH,DH2}$=
431 1.3 x 10^{10} M^{-1} for the second step. By considering the binding sites to be non-interacting with
432 each other, we can further assess these constants in terms of a two-step binding, Adair
433 binding equation[55] to evaluate the intrinsic hemin affinity per subunit. In this case, the
434 intrinsic hemin affinity per subunit for the first step is $1/2K_{D,DH}$ or 6.5 x 10^{10} M^{-1}, and the intrinsic
435 affinity per subunit of the second step is $2K_{DH,DH2}$ or 2.6 x 10^{10} M^{-1}. This ~3 –fold decrease in
436 hemin affinity could be due to either negative cooperativity or differences in hemin binding to
437 the α versus β subunits. The non-cooperative, subunit differences interpretation is the most
438 reasonable because we and others [22, 38-40] have already shown that the rate of hemin
439 dissociation from β subunits is higher than α subunits in metHbA. Therefore, in our model,
440 these intrinsic hemin affinities can be interpreted to indicate that the initial loss of hemin from
441 the native folded dimer comes from the β subunit generating the semi-holo DH state with
442 hemin still in the α subunit.

443 Hemin binding to the molten globule dimer for HbA also occurs sequentially, and in this
444 case, the differences in hemin affinity between the first and second steps is even larger, with
445 $K_{I,IH}$ = 1.1 X 10^{11} M^{-1} and $K_{IH,IH2}$= 3.3 x 10^{8} M^{-1} (Table 1). In this case, the intrinsic subunit
446 affinity for the first step is $1/2K_{I,IH}$ =5.5 x 10^{10} M^{-1} and almost equal to that for the first step in
447 hemin binding to the native D state. In contrast, the intrinsic affinity for the second step is only
448 $2K_{IH,IH2}$ =6.6 x 10^{8} M^{-1}. Again, this significant decrease in affinity suggests the subunit
449 differences in the folded state increase ~30-fold in the molten intermediate. Based on the
450 known higher hemin loss rates from the β subunit in the folded states [22, 38-40], it appears
451 likely that its affinity for hemin is even lower in the molten or hemichrome I state.

452 The unfolded apo- and holo monomers at high [GdnHCl] only have residual α-helical
453 content, ranging between ~10 % and 20 % relative to folded HbA subunits (Table 1) [4]. Thus,
454 as expected, the fitted hemin affinity for these unstructured monomers is small $K_{U,UH}$= 2.9 x 10^7
455 M^{-1} (Table 1) and likely dominated by non-specific interactions [9, 11, 42, 43] (Table 1).
456 As shown in Figure 4, we were also able to analyze successfully holoHbF unfolding
457 data with the same Model 1. In this case, a somewhat higher $\chi 2$ value of 1.76 was obtained. In
458 folded dimers, the hemin affinity for the first and second steps in hemin binding were more
459 similar with $K_{D,DH}$= 2.5 x 10^{11} M^{-1} (intrinsic subunit affinity, 1.3 x $10^{11}M^{-1}$) and $K_{DH,DH2}$= 1.3 x
460 10^{11} M^{-1} (intrinsic subunit affinity, 2.6 x $10^{11}M^{-1}$) indicating non-cooperative binding and little or
461 no subunit differences. However, the affinities of the first and second steps for binding to the
462 HbF molten intermediate were quite different, with $K_{I,IH}$ = 7.8 X 10^{11} M^{-1} (intrinsic subunit
463 affinity, 3.9 x 10^{11}) and $K_{IH,IH2}$= 1.4 x 10^9 M^{-1}(intrinsic subunit affinity 2.8 x 10^9 M^{-1}). Again, it
464 seems that the γ subunits have much lower hemin affinity in the molten globule intermediate.
465 The U monomers for HbF also had ~10-fold higher hemin affinity than in HbA, and the holo
466 monomers, UH had slightly higher α-helical content at 30% relative to folded HbF (Table 1).
467 Regardless of the exact interpretation, it is clear that one of the hemichrome containing
468 subunits in the molten dimer states of both HbF and HbA has an affinity for hemin that is
469 similar to that in the folded D state.
470

471 **Modeling HbA disassembly in erythrocytes and in blood plasma**

472 During maturation of red blood cells, all of the membrane organelles in the cytoplasm,
473 including the nucleus and mitochondria, are eliminated to allow for dense packing of
474 hemoglobins to a concentration of ~20 mM per subunit [56-58]. At these high concentrations,
475 native oxyhemoglobin exists almost completely as holo tetramers because the tetramer-dimer

476 disassociation constant ($K_{4,2}$ or $1/K_{2,4}$) is on the order of 10^{-6} M, and the corresponding value
477 for deoxyhemoglobin is even lower on the order of 10^{-12} M [49, 59, 60].

478 If oxidative stress occurs in erythrocytes due to either genetic disorders or
479 environmental chemicals or drugs, denaturation of the resultant metHb can occur in the cell
480 cytoplasm. At these high hemoglobin concentrations, the major disassembly pathway will be
481 dominated by holoprotein disassembly intermediates, represented by the left side of Figure 1.
482 To illustrate this effect quantitatively, we computed the population fractions of all the
483 intermediates for a GdnHCl-unfolding titration at 20 mM total protein using the parameters in
484 Table 1 (Figures 6A and B). The initial step involves dissociation of holo tetramers into holo
485 dimers, which is followed by unfolding into molten holo dimers with hemichrome spectra. This
486 IH_2 species is the dominant intermediate with small amounts of the semi–holo molten globule,
487 IH. The IH_2 and IH species dissociate directly into unfolded holo monomers before any
488 significant hemin loss occurs. The high Hb subunit concentration inhibits dissociation of both
489 the dimeric intermediates and bound hemin. Even the loss of hemin bound weakly to unfolded
490 monomers is inhibited until very high [GdnHCl]. When model 2 and the parameters in
491 Supplement Table 1 are used to simulate the population fractions at 20 mM Hb, the same
492 conclusion on the dominant role of holoprotein intermediates is reached (Figure Supplement
493 3A and 3B).

494 Hemolysis of red cells leads to the release of hemoglobin into blood plasma and can be
495 triggered by hemoglobinopathies, red cell aging, oxidative stress, blood infections by heme
496 iron extracting pathogens, and complications during cardiovascular medical procedures and
497 blood transfusions. Dilution into the large volume of plasma leads to very low, micromolar Hb
498 concentrations, which causes almost complete disassociation of tetrameric Hb into dimers and
499 accelerates auto-oxidation [23, 61-66]. Thus, when hemoglobin is diluted into plasma after red
500 cell lysis, metHb formation occurs and dissociation of both the inter-subunit interfaces and

501 hemin are facilitated. This situation was simulated in Figures 6C and D using the parameters in
502 Table 1 and 0.5 μM total protein. The disassembly pathway is quite different from that in red
503 cells. The initial holoprotein is primarily a dimer, DH_2 (Figures 6C) and the dominant
504 intermediates are the semi-holo molten dimer, IH, and the apo unfolded U monomer until the
505 completely unfolded chains, U_C are formed. Perhaps the most striking difference between the
506 red cell versus plasma pathways is the early appearance of free hemin before unfolding is
507 finished (Figure 6D). At low Hb concentration, dissociation of the $\alpha_1\beta_1$ dimer interface is
508 facilitated, resulting in low populations of the molten dimer hemichromes. Hemin dissociation is
509 also facilitated, leading to predominately apo intermediates and unfolded chains even before
510 the end of the simulated titration.
511

512 **Small angle X-ray scattering (SAXS) analysis of apoHb properties in solution relative to**
513 **holoHb**

514 SAXS intensity measurements (Figure 7) were done on both apo- and holo forms of the
515 recombinant crosslinked HbA or rHb0.1, which has a single-residue glycine linker covalently
516 connecting the N-terminal of the first α_1 subunit to the C-terminal of the second α_2 subunit. The
517 linker causes the aporHb0.1 to remain as a tetramer under conditions where native apoHb is a
518 dimer [4]. We chose the aporHb0.1 variant for SAXS analysis in order to have a covalently
519 crosslinked tetramer as standard for evaluating the radius of gyration (R_g) for holoHb
520 tetramers. The SAXS measurements were also done on the holo forms of the corresponding
521 non-crosslinked recombinant HbA, known as rHb0.0 [67-69]. Both rHb0.0 and rHb0.1 have a
522 V1M mutation in each subunit to initiate protein expression [4]. The SAXS measurements were
523 fitted to the Guinier plot equations (Figure 7 inset) to obtain R_g for each molecule. Minor effects
524 of molecular crowding were only observed for apoHb, occurring at protein concentrations >1.5
525 mg/ml (Figure supplement 4). Therefore for aporHb0.1, R_g and the pair distance distribution

526 function P(r) between atoms was determined with SAXS scattering measurements
527 extrapolated to infinite dilution in order to remove the molecular crowding effects [70] (Figure
528 7,Supplement Figure 4, and Supplement Figure 5). AporHb0.1 at 0.0 mg/ml exhibited a R_g of
529 ~29.4 Å, whereas for the holo forms of rHb 0.0 and rHb0.1, the experimental R_g values
530 calculated were within the R_g range of 24 Å, as expected from the known crystal structure of
531 holoHbs (e.g. PDB ID 1O1L) (Figures 7 and supplement 4). Thus, aporHb0.1 is expanded in
532 solution. These kinds of expansions are often observed for partially unfolded proteins [70], and
533 support our view that hemin dissociation causes loss of the ability of hemoglobin to form
534 compact and cooperative tetramers. The losses of helical content are likely occurring around
535 the heme cavity regions, which also forms the tetramer interface, allowing expansion of the
536 crosslinked protein.

537 Interestingly, our SAXS measurements also suggest that this loss of helical content due
538 to hemin dissociation increases the susceptibility of Hb to molecular crowding. Similar effects
539 of molecular crowding probably might occur for the partially disordered assembly intermediates
540 and during early folding events for Hb in vivo. With more sticky regions of unfolded chain
541 segments exposed and expanded in solution, there is also a higher probability they can come
542 in closer contact and even interact weakly with other protein molecules causing the crowding.
543

544 Discussion

545 Global disassembly pathway for human hemoglobin

546 Hetero-tetrameric hemoglobins evolved from monomeric vertebrate myoglobins within
547 the globin metalloprotein family about 600 millions ago [1, 71, 72]. In this work, we have
548 shown for the first time that human hemoglobin shares a common disassembly pathway with
549 mammalian myoglobin. For both systems, hologlobin disassembly is mediated via a molten
550 hemichrome intermediate. However, relative to the simpler myoglobin monomer system

551 described in [11], the human hemoglobin assembly/disassembly mechanism evolved to be
552 much more complex. This complexity is demonstrated by the multiple steps for heme binding
553 to dimeric intermediates and by the sequential formation of the dimer ($\alpha 1\beta 1$) and then tetramer
554 ($\alpha 1\beta 2$) interfaces (Figure 1).

555 To best of our knowledge, no one has previously tried to analyze reversible holoHb
556 disassembly quantitatively with a comprehensive model because of its complexity. In addition,
557 most studies involved thermal denaturation [73-75], which leads to precipitation of both the
558 globin chains and free hemin in conventional buffers. Our study has also been the first attempt
559 to measure equilibrium hemin binding parameters for hemoglobin, and provides reasonable
560 estimates for comparison with previous kinetic studies [22, 74, 76]. We were also able to
561 estimate heme binding parameters at different stages of Hb assembly/disassembly,
562 independently, and characterize how they influence inter-subunit assembly and globin folding.
563 Determination of hemin affinity constants is not possible by direct titration of apoglobins with
564 hemin because free hemin stacks to form dimers and higher molecular weight aggregates
565 even in the micromolar region [46]. In our experiments, the hemin equilibrium binding
566 constants were obtained by simultaneously analyzing GdnHCl-induced unfolding curves for
567 both apo- and holoHb in order to avoid problems associated with apoglobin and hemin
568 precipitation.

569 Hargrove, Barrick, and Olson [74, 76] had previously concluded that the rate constant
570 for hemin binding to apoglobin seems to be relatively invariant and $\approx 1 \times 10^8\ M^{-1}\ s^{-1}$ per subunit
571 regardless of the globin structure for either apoHb or apomyoglobin. Past kinetic studies were
572 focused mostly on measuring heme disassociation rates from the end-state products of Hb
573 assembly e.g. TH_4,TH_2, and DH_2 (Figure 1) [22, 77]. However, such kinetic studies did not
574 attempt to consider how these rates and hemin affinities change as unfolding proceeds via
575 molten globules with significant reconfigurations of the hemin pockets.

576 The approaches that led us to successfully resolve “new” holo disassembly
577 intermediates in the model in Figure 1 and then determine their roles were (1) deconvolution of
578 visible absorbance signals into various intermediate hemin containing populations; (2) model
579 fitting to both apo- and holo protein unfolding spectral measurements; and (3) examination of
580 the protein concentration dependency of bimolecular events involving both inter-subunit
581 interactions or heme binding. We also developed a model evaluation approach that
582 incorporates numerical analysis methods to solve for the total disassembly population by
583 addressing the complexity of the Hb protein with four subunits and four bound hemin
584 molecules. For monomeric heme proteins, more straightforward quadratic equations can be
585 used to solve for fractions of various holo- and apo intermediates [11, 44].
586

587 **Physiological relevance**

588 The results in Figures 6A and B can also provide insights for the assembly pathway at
589 various protein and heme concentrations during hemoglobin biosynthesis. First, hemin binding
590 is a bimolecular process and required for tetramer assembly. Therefore, at high heme and
591 protein concentrations, the fraction of the holo molten globule and native dimers will
592 outcompete their apo counterparts to promote tetramer formation. In addition, at these high
593 concentrations, weak hemin binding to U monomers might be interpreted as an induced fit
594 mechanism [5], promoting holoprotein assembly from newly expressed α and β chains in
595 immature red blood cells or reticulocytes. This prediction seems to fit with previous
596 observations by Spirin's group [78] which suggest co-translational heme binding to nascent
597 globins chains coming off the ribosome in cell-free lysates of rabbit reticulocytes where high
598 concentrations of hemin were added [78]. Alternatively, at much lower concentrations of Hb
599 subunits and free hemin, hemin binding during assembly will proceed through conformational
600 selection[5] of specific partially or fully-folded conformations (Figures 6C, 6D). Even though the

601 total amount of holoHb being generated during erythropoiesis is large, the absolute
602 concentrations of the newly synthesized apo chains and free hemin in the steady state are
603 likely to be much lower due to rapid Hb assembly and hemin sequestering in membranes and
604 carrier proteins[79]. In addition, if unfolded globin chains and free hemin were present at high
605 concentrations, they would self-aggregate rapidly to form protein precipitates and stacked
606 hemin complexes[46], which would compete with assembly, causing unwanted pathological
607 situations.

608 We do acknowledge that our disassembly model derived from *in vitro* studies cannot
609 completely capture *in vivo* disassembly/assembly mechanisms. Within the packed red-cells,
610 non-specific or quinary interactions[80, 81] will occur between different combinations of α and
611 β chains for formation of transient U_2 species (Figures 6B) [4]. Our previous *in vitro*
612 experiments have shown that transient aggregation to generate apo U_2 intermediates actually
613 dampens the dimer formation [4]. Although these interactions could facilitate the correct
614 orientations for hetero-dimer assembly, such non-specific interactions could also potentially
615 lead to inclusion bodies in red cells. The later is especially likely if the subunit concentrations
616 are unequal and result in homo-oligomers (e.g. α_n or β_n occurring during thalassemia diseases)
617 due to disrupted expression or genetic instability of either α or β subunits [20]. *In vivo*
618 experiments are further needed to investigate how these non-specific interactions and
619 molecular crowding influence the $\alpha_1\beta_1$ dimer formation during Hb biosynthesis.

620 Finally, hemichromes are often observed within inclusion or Heinz bodies in red cells
621 [12, 17]. These particulates are found in red cells with hemoglobinopathies associated with
622 globin instability or oxidative stress. The results in Figures 6A and 6B provide an explanation
623 for the presence of these species. At the high internal hemoglobin concentration in red cells,
624 the unfolded holoprotein intermediates are dominant, leading to a much higher probability of
625 misassembled Hb being trapped in the large hemichrome populations for the UH or IH_2 states.

626 Our model was developed to examine unfolding as function of GdnHCl denaturant
627 concentrations but could be modified to include other environmental or physiological Hb
628 disassembly triggers such as lower pH or higher temperatures. Additionally, we can use the
629 population fraction values extrapolated to 0 M GdnHCl to estimate the relative absolute free
630 energies of different folding species *in vivo* as $-RTlnY_i$ for species i, where a large positive
631 value indicates a very unstable state (Figure 8). These values suggest the amount of free
632 energy that has to be added to disassemble or unfold the globin to a particular state. Figure 8
633 shows that the free energy differences between apo- and holo intermediates are predicted to
634 be higher in the red cells compared to dilute plasma environments where hemin and subunit
635 dissociation is promoted. However, in both environments the holo- and semi-holo disassembly
636 intermediates are generally favored over the apo variants.

637 When not contained within the reductive environment of red cells, acellular hemoglobin
638 in plasma undergoes rapid autooxidation forming metHb, which in turn enables rapid heme
639 disassociation. NO, which is generated in endothelial cells to facilitate vasodilation, can also
640 react with acellular oxyHb to produce metHb and nitrate. A surge of acellular Hb in the
641 bloodstream can lead to vasoconstriction due to NO scavenging by this dioxygenation reaction
642 and subsequent release of hemin from acellular metHbA [63, 82-86].

643 The early onset of a significant population of disassociated free hemin in the low protein
644 concentration pathway (Figures 6C and 6D) provides an explanation for why chronic or severe
645 hemolysis triggers free hemin mediated inflammatory diseases and endothelial dysfunctions
646 that lead to serious cardiovascular complications and kidney problems [61, 87, 88]. The
647 disassociated free hemin intercalates into cell membranes and leads to the generation of
648 reactive oxygen species (ROS) that can damage lipid, protein, and DNA [82, 89]. Free hemin
649 can also bind specifically to the toll-like receptor-4 (TLR4) on endothelial cells, triggering
650 adverse pro-inflammatory cell cascades [90, 91]. Hemin-mediated ROS generation and

651 oxidative stress on the blood vessel walls also promotes adhesion molecule expression on the
652 walls, leading to platelet aggregation and thrombosis [61, 82].
653

654 Conclusion

655 We have been able to derive for the first time a quantitative Hb disassembly/assembly
656 model, which can be used as a framework to identify the factors that resist Hb denaturation
657 and those that enhance expression. The key feature of our model involves formation of molten
658 globule intermediates with hemichrome spectral properties, and these intermediates are part of
659 the pathway for the disassembly and unfolding of native hemoglobin. Complementary
660 computational studies are also being done in our group to expand this framework to include
661 interpretations at an atomic level. Hopefully, our efforts to obtain a comprehensive mechanism
662 of Hb disassembly will lead to strategies for addressing erythropoiesis disorders and
663 hemoglobinopathies in a clinical setting and for engineering more stable acellular hemoglobin-
664 based oxygen carriers for transfusion therapy.
665

666 Materials and Methods

667 Cloning, expression and purification of Hb variants

668 The molecular biology and protein purification workflow for preparation of holoHb
669 samples were described in our previous paper on apoHb unfolding (see [4] and references
670 therein). Native HbA was extracted from expired blood units (Gulf Coast Regional Blood Bank,
671 Houston, TX). Recombinant native HbA and HbF were co-expressed with *E. coli* Met
672 aminopeptidase from pHE2 and pHE9 E. coli expression plasmids, respectively, in JM109
673 E.coli cells (Promega) as described by [92, 93]. The plasmids were a gifts from Dr. Chien Ho's
674 research group (Carnegie Mellon University). The aminopeptidase cleaves post-translationally

675 the initiator Met residue preceding the V1 residue in each Hb subunit. Recombinant HbA
676 variants with αH58L/V62F and βH63L/V67F mutations were then constructed through site
677 directed mutagenesis using Agilent QuckChange® Lightning Kits. rHb0.0 and rhHb0.1 were
678 expressed from pDL111-13e and pSGE1.1-E4 expression plasmids respectively in SGE1661
679 E.coli cells [67-69]. These cells and both plasmids were gifts from Somatogen Inc. (later Baxter
680 Hemoglobin Therapeutics).

681 Protein expression in cells was induced by 0.2 mM isopropyl β-D-1-
682 thiogalactopyranoside with the cells either grown in 500 ml terrific broth in flasks for medium-
683 scale recombinant Hb expression following protocols developed by Ho's group [92, 93] or in a
684 Biostat C 20 bioreactor for large scale expression followed protocols developed initially by
685 Somatogen, Inc. [68] and then modified by our group [94]. Isolation and purification of native
686 HbA and the recombinant hemoglobins were done as described by [68, 92-94]. Cell lysates
687 containing Hb were initially purified using a Zn^{2+} charged chelating Sepharose Fast Flow resin
688 column (GE healthcare) because Hb surfaces are rich with His residues that can bind Zn^{2+}
689 (also see [95]). Further Hb purification was done using a Q Sepharose anion exchange column
690 (GE healthcare), and a final purification step was done for the Hbs expressed from the pHE2
691 and pHE9 plasmids using a S Sepharose cation exchange column (GE healthcare) to
692 eliminate Hbs with uncleaved initiator Met residues. Quality and identify of the purified Hbs
693 were confirmed by: visible absorbance spectra for oxygenated, CO bound, and metHb forms;
694 electrospray ionization time-of-flight mass spectrometry; and reverse phase high performance
695 liquid chromatography (Agilent 1220 Infinity LC system) analyses [69, 96]. All hemoglobin
696 samples were purified and stored in their reduced CO forms to prevent auto-oxidation by
697 flushing cell lysates, purified proteins, and all the buffers with pure CO for ~30 minutes [97, 98].
698

699 **Preparation of metHb, apoHb, and hemichrome standards**

700 MetHb was prepared by oxidizing HbO_2 sample with a slight excess of potassium
701 ferricyanide. HbO_2 was initially prepared by flushing of HbCO samples with pure O_2 for ~30
702 minutes in chilled rotating flask that was exposed to an intense industrial light to promote
703 photodissociation of the bound CO [21, 97, 99].
704 ApoHb was prepared from the metHb according to the method developed by Antonini's
705 group [100]. First, the pH of a concentrated metHb sample was quickly reduced to ~2.2
706 followed by extraction of disassociated hemin into cold 2-butanone. Apoglobin recovered from
707 the extraction was then buffer exchanged into 10 mM potassium phosphate, 1mM DTT at pH
708 7. All ApoHb and metHb samples were prepared and examined at ~ 4 °C [4].
709 Hemichrome standards were prepared in order to obtain their reference spectra (Figure
710 2B). Excess imidazole was added to 12 μM HbA to allow for the binding of imidazole to the
711 hemin iron atom, thereby mimicking the hemin electronic structure of a *bis*-histidine
712 hemichrome. The visible absorbance spectra obtained from this species overlapped with the
713 hemichrome spectra generated by the addition of 600 μM sodium dodecyl sulfate, a
714 denaturant, to the same amount of HbA[11, 26, 48, 101].
715
716 **Measurements of holoHb unfolding**
717 MetHb samples were prepared in varying concentrations of GdnHCl in 200 mM
718 potassium phosphate, pH 7. The samples were incubated for 1 hour in a water bath at 10 °C.
719 Spectroscopic measurements of unfolding were then recorded at 10 °C in order to maintain the
720 solubility of unstable folding intermediates. These experimental protocols closely follow our
721 previous apoHb equilibrium unfolding measurements, except that for the addition of 1mM DTT.
722 DTT was added to the apoglobin samples to prevent formation of non-native, disulfide bonds
723 which occur during the preparation and storage of apoHb [4]. In our work with metHb samples,
724 DTT was observed to cause partial reduction, large visible absorbance changes, and a

725 complicated mixture of oxidation states, including deoxyHb and HbO_2. Thus, DTT was not
726 added to samples for holo- metHb unfolding experiments.

727 The CD and hemin absorbance changes were reversible when holoHb samples
728 incubated in concentrated GdnHCl solutions were diluted to reduce the extent of disassembly
729 and unfolding. CD spectral changes were measured using a Jasco J-810 CD
730 spectropolarimeter, and visible absorbance measurements were measured using a Cary 100
731 Bio UV-Visible spectrophotometer [4, 97]. During the CD spectra data collection, scanning
732 speed was set to 100 nm/min, data pitch was set to 0.1 nm, data integration time was set to 1
733 sec, and spectral bandwidth was set to 1 nm. For the visible absorbance data collection, data
734 interval was 1 nm. Blank buffer solutions were measured initially to enable baseline corrections
735 to be done on the spectral measurements with the spectrophotometer and spectropolarimeter
736 softwares. For a small portion of the visible spectral measurements recorded, baseline drifts
737 were observed. For each of the spectra with baseline drift, a new baseline was linearly
738 interpolated, using MATLAB R2017a (The MathWorks, Inc., Natick, MA), from the first 21
739 points of each spectrum at the longest wavelengths. The new baseline was then subtracted
740 from the corresponding spectrum.

741 Visible absorbance spectra at each [GdnHCl] were analyzed in terms of population
742 fractions of folded metHb, hemichrome species, and free hemin, using standard basis spectra
743 (B_i) for each species I (Figure 2B). The standard basis spectra for folded recombinant metHb
744 α(H58L/V62F)β(H63L/V67F) is different from that of aquametHbA because of the absence of
745 the H_2O ligand at the hemin iron [102]. For the mutant relative to aquametHbA, the Soret peak
746 is blue-shifted to 400 nm and the smaller peak at 630 nm is shifted to 600 nm (Figure
747 Supplement 6).

748 For all the visible absorbance deconvolutions, the fmincon minimizer in MATLAB
749 R2017a (The MathWorks, Inc., Natick, MA) was used to minimize squared residual difference

750 between the absorbance model defined in eq 9 and the measured experimental visible
751 absorbance spectrum in order to determine the population fraction (D_i) of each species.

752 $$\text{Absorbance model} = \left(B_{\text{MetHb}}\right) x D_{\text{Folded metHb}} + \left(B_{\text{Hemichrome}}\right) x D_{\text{Hemichrome}} + \left(B_{\text{Free hemin}}\right) x D_{\text{free hemin}}$$

753 eq 9

754

755

756 **SAXS sample preparations, measurements, and data analysis**

757 Analytical gel filtration was used to verify whether samples were mono-disperse. Holo-
758 and apoHb samples were prepared by thorough buffer exchange into degassed 10 mM
759 potassium phosphate, pH 7, 5 mM DTT. The buffer was degassed and contained DTT to
760 prevent during data collection error causing bubble formation and radiation damage (RAD) of
761 protein. HoloHb samples were also kept in the CO bound form to further inhibit heme
762 autoxidation during data collection[97, 103, 104].

763 SAXS measurements of the Hb samples were done using the Rigaku Bio-SAXS 1000
764 instrument at the Sealy Center for Structural Biology and Molecular Biophysics at the
765 University of Texas Medical Branch at Galveston, TX. Data were collected at 10 °C, with 12 to
766 16 hours of exposure to X-ray radiation, monitored hourly for RAD. SAXS measurements of
767 buffer alone were also done to enable blank subtraction. Data collection was done at varying
768 protein concentrations, ranging from 1mg/ml to 6 mg/ml. SAXSLab software (Rigaku) was
769 used for data collection, the SAXNS webserver (http://xray.utmb.edu/saxns) was used for
770 buffer subtraction, and the ATSAS software suite was used for data analysis. From within the
771 ATSAS software, PRIMUS, almerge, and CRYSOL packages were used for preparation and
772 analysis of the observed X-ray scattering curves and GNOM was used to generate P(R) plots
773 [97, 105].

774

775

776 ## Additional Supplementary Files

777 The following additional figures and table are compiled together in the Supplement.pdf file

778 included.

779 **Figure supplement 1.** Comparison of GdnHCl-induced equilibrium unfolding measurements of

780 holo- HbA, HbF, rHb0.1, and Hb α(H58L/V62F)β(H63L/V67F)

781 **Figure supplement 2.** Fittings of holoHbA GdnHCl-induced disassembly measurements to

782 HbA equilibrium disassembly model 2

783 **Figure supplement 3.** Simulated HbA disassembly population fractions in Hb packed red

784 blood cells and dilute blood plasma

785 **Figure supplement 4**. The Guinier Plots of each Hb dilution series

786 **Figure supplement 5.** The GNOM P(r) plots for aporHb0.1, holorHb0.1, and holorHb0.0

787 **Figure supplement 6**. Visible absorbance spectra for metHb α(H58L/V62F)β(H63L/V67F)

788 **Table supplement 1**. Fitted equilibrium disassembly parameters to model 2 for HbA

789

790 **Abbreviations**

791 GdnHCl, guanidine hydrochloride; Hb, hemoglobin; HbA, adult human hemoglobin A; HbF,

792 fetal human hemoglobin; metHb, oxidized hemoglobin with heme iron in the Fe^{3+} form; apoHb,

793 hemoglobin with the heme removed; rHb, recombinant hemoglobin; Mb, myoglobin; $K_{2,1}$,

794 heterodimer equilibrium dissociation constant; $K_{4,2}$, tetramer equilibrium dissociation constant;

795 CD, circular dichroism; DTT, dithiothreitol; rHb0.0, recombinant hemoglobin with V1M

796 mutations in both α and β globin chains; rHb0.1, recombinant hemoglobin with V1M

797 mutations in both di-α and -β globin chains and a single glycine linker joining the C-terminus

798 of the first α chain and the N-terminus of the second α chain; MALDI-TOF, matrix-assisted

799 laser desorption ionization time-of-flight; HPLC, high-performance liquid chromatography;

SDS, sodium dodecyl sulfate.

Acknowledgements

We would like to thank Thomas Grant for reviewing our SAXS data and analyses and Jayashree Soman and Eileen Singleton for help in expressing, purifying, and running quality control analyses of many of the recombinant hemoglobins.

Authors' contributions

PPS helped design the study, performed all the experiments, analyzed all of the data, and wrote all the drafts of the paper. The experiments were part of her Ph.D. thesis at Rice University under the guidance of JSO and GNP. She finalized the holoHb disassembly model and analyses at Rutgers University with the support of DAC. MAW performed and analyzed the SAXS experiments with samples provided by PPS. WCO expressed and purified the HbF samples and performed several HbF unfolding experiments as part of his undergraduate thesis at Rice University. GNP helped guide the work and edit various drafts of the paper. DAC also edited the paper and focused the modeling work on medical and physiological relevance. JSO helped to design the in vitro folding experiments, provided initial ideas about the model and analyses, and was the major editor of the manuscript.

Funding

The research reported in this paper was funded by National Institutes of Health Grants HL110900 (JSO.) and GM109456 (GNP), the BioXFEL Science and Technology Center Grant NSF 1231306 (GNP), the BioXFEL Science and Technology Center Grant NSF 1231306 (DAC and PPS), Grant C-0612 from the Robert A. Welch Foundation (JSO and PPS), and the Sealy Center for Structural Biology and Molecular Biophysics at UTMB.

825

826

827

828 **Availability of data and materials**

829 The data sets used in the unfolding analyses are available from the corresponding author on
830 reasonable request. Some of the protein samples and plasmids for the various Hbs are also
831 available but the amounts are limited because of the retirement of JSO.

832

833 **Ethics approval and consent to participate**

834 Not applicable

835

836 **Consent for publication**

837 Not applicable

838

839 **Competing interests**

840 The authors declare that they have no competing research or financial interests in this work.

841

842 Figure titles and legends

843 Figure 1. **Equilibrium disassembly models of HbA** A. **in cell and** B. **in vitro**. Model 1 is the
844 blue section and model 2 is the black and blue sections combined. In A, free hemin is the
845 green symbol, and bound hemin is the red symbol. Initially, the holoHb tetramer (TH_4)
846 disassociates into holoHb dimers (DH_2). Alternatively, TH_4 can undergo hemin (H)
847 disassociation from the subunits with lower hemin affinity to form the semi holotetramers (TH_2).
848 DH_2 can also undergo H disassociation sequentially first to form semi holo-dimers (DH),
849 followed by further H disassociation leading to apoHb (D) formation. DH_2 unfolds into holo-

850 molten globules (IH_2) with hemichromes characteristics. IH_2 also can lose H sequentially first
851 to form semi holo- molten hemichromes followed by formation of the apo- molten intermediates
852 (I). IH_2 next disassociates and simultaneously unfolds into holomonomers (UH). Loss of H from
853 UH leads into apo-monomers (U) with residual helical content. U can either associate non-
854 specifically with each other to form transient unfolded dimers (U_2) or completely unfold into
855 polypeptide chains (U_C). The apoHb unfolding mechanism had been derived independently in
856 our previous study[4].
857
858 Figure 2. **Visible absorbance spectra measurements for HbA disassembly**. A.
859 aquametHbA disassembly induced by GdnHCl; and B. aquametHbA, hemichrome, and free
860 hemin at 12 μM per subunit protein concentration. Unfolding measurements in 2A panel were
861 done at 12 μM per subunit total protein concentration. All holoHb unfolding measurements
862 were done in 200 mM potassium phosphate (pH 7) at 10 °C. Protein samples were initially
863 prepared in aqua-met oxidation states.
864
865 Figure 3. **Fittings of holoHbA GdnHCl-induced disassembly measurements to HbA**
866 **equilibrium disassembly model 1**. The solid circles are the measured data at different per
867 subunit total protein concentration, the solid lines are the fits, and the dashed lines are the
868 theoretical population fraction of folded holoHbA tetramers (TH_4) derived from the fittings. A.
869 Population fractions of aquamet- holoHb dimers and tetramers. B. Population fractions of
870 hemichromes. C. Population fractions of free hemin. D. Fractional CD change at 222 nm, a
871 measure in the change of alpha-helical structure content relative to folded holoHbA. The
872 apoHbA unfolding measurements (curves at the far left) were obtained from previously
873 published data[4]. The experimental measurements in A-C panels were obtained from
874 deconvolution of visible absorbance spectra recorded between 350 nm and 660 nm. All holoHb

875 unfolding measurements were done in 200 mM potassium phosphate (pH 7) at 10 °C. Protein
876 samples were initially prepared in aqua-met oxidation states. Each data point is an average of
877 triplicate titrations of protein with denaturant.
878
879 Figure 4. **Fittings of holoHbF GdnHCl-induced disassembly measurements to HbA**
880 **equilibrium disassembly model 1**. The solid circles are the measured data at different per
881 subunit total protein concentration, solid lines are the fits, and dashed lines are the theoretical
882 population fraction of folded holoHbF tetramers (TH_4) derived from the fittings. A. Population
883 fractions of aquamet- holoHb dimers and tetramers. B. Population fractions of hemichromes.
884 C. Population fractions of free hemin. D. Fractional CD change at 222 nm, a measure in the
885 change of alpha-helical structure content relative to folded holoHbF. The experimental
886 measurements in A-C panels were obtained from deconvolution of visible absorbance spectra
887 recorded between 350 nm and 660 nm. All holoHb unfolding measurements were done in 200
888 mM potassium phosphate (pH 7) at 10 °C. Protein samples were initially prepared in aqua-met
889 oxidation states. The 12 μM Hb CD unfolding measurement was obtained from previously
890 published data [4].
891
892 Figure 5. **Comparison of GdnHCl-induced equilibrium unfolding measurements of holo-**
893 **HbA, HbF, rHb0.1, and Hb α(H58L/V62F)β(H63L/V67F).** The solid circles are the measured
894 data at 12 μM per subunit total protein concentration. A. Population fractions of met- holoHb
895 dimers and tetramers. B. Population fractions of hemichromes. The experimental
896 measurements were obtained from deconvolution of visible absorbance spectra recorded
897 between 350 nm and 660 nm. All holoHb unfolding measurements were done in 200 mM
898 potassium phosphate (pH 7) at 10 °C. Protein samples were initially prepared in met oxidation
899 states.

900 Figure 6. **Simulated HbA disassembly population fractions** in A. **Hb packed red blood**
901 **cells and** B. **dilute blood plasma** demonstrate Hb concentration directed disassembly
902 pathways. Simulations were done using Model 1 (Figure 1) and the parameters in Table1 as a
903 factor of GdnHCl.
904
905 Figure 7. **SAXS Log intensity profiles and Guiner plot (inset) for recombinant**
906 **hemoglobins.** For the Log-Log plots, the samples shown are the zero-concentration
907 extrapolated aporHb0.0 (green), 2.0 mg/ml Hb0.1 (blue) and 2.0 mg/ml Hb0.0 (red) Inset: The
908 Guinier plots with their residuals (darker lines) and ($1.3/R_g$) Guinier q-upper limits (dashed lines
909 for R_g=29.4, 24.3, 23.6 Å). The expansion of the apoprotein is obvious from the less distinct
910 minima in the higher angle data.
911
912 Figure 8. **Predicted relative free energies of various Hb disassembly intermediates** in A.
913 red cells and B. diluted into plasma**.**
914
915
916 **Figures**

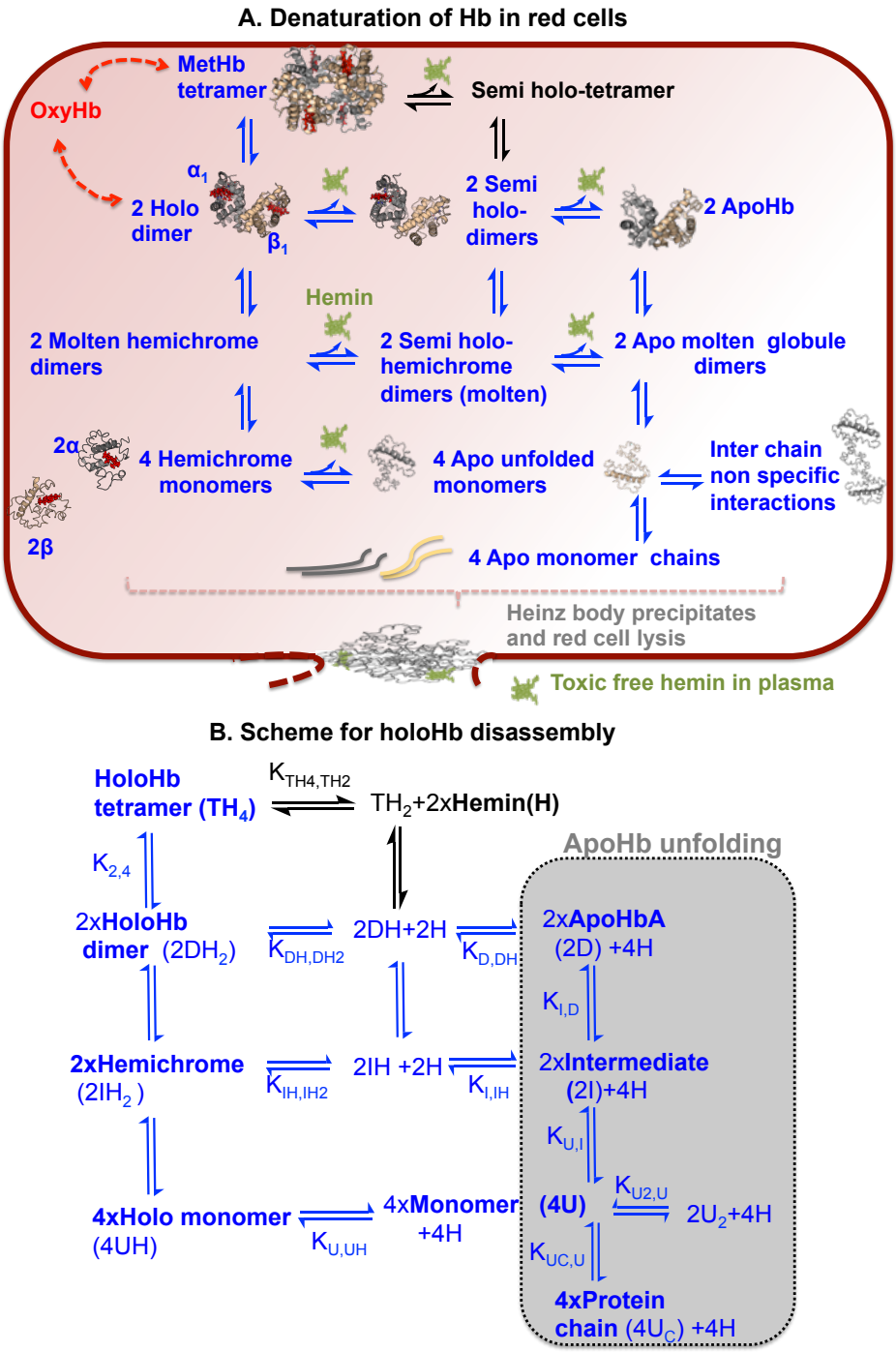

Figure 1. **Equilibrium disassembly models of HbA** A. **in cell and** B. **in vitro**. Model 1 is the blue section and model 2 is the black and blue sections combined. In A, free hemin is the green symbol, and bound hemin is the red symbol. Initially, the holoHb tetramer (TH_4) disassociates into holoHb dimers (DH_2). Alternatively, TH_4 can undergo hemin (H) disassociation from the subunits with lower hemin affinity to form the semi holotetramers (TH_2). DH_2 can also undergo H disassociation sequentially first to form semi holo-dimers (DH), followed by further H disassociation leading to apoHb (D) formation. DH_2 unfolds into holo-molten globules (IH_2) with hemichromes characteristics. IH_2 also can lose H sequentially first to form semi holo- molten hemichromes followed by formation of the apo- molten intermediates (I). IH_2 next disassociates and simultaneously unfolds into holomonomers (UH). Loss of H from

UH leads into apo-monomers (U) with residual helical content. U can either associate non-specifically with each other to form transient unfolded dimers (U_2) or completely unfold into polypeptide chains (U_C). The apoHb unfolding mechanism had been derived independently in our previous study[4].

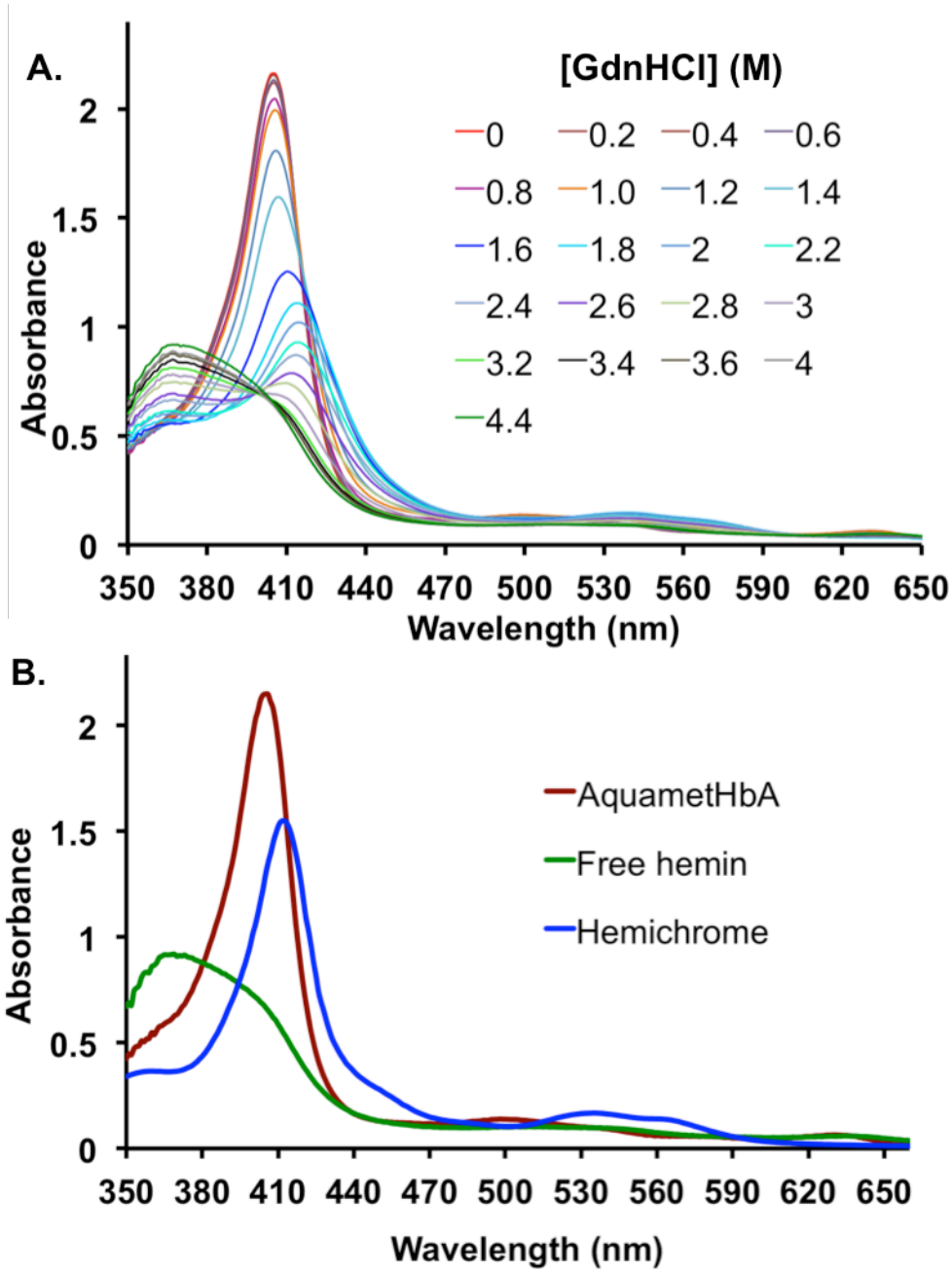

Figure 2. **Visible absorbance spectra measurements for HbA disassembly**. A. aquametHbA disassembly induced by GdnHCl; and B. aquametHbA, hemichrome, and free hemin at 12 μM per subunit protein concentration. Unfolding measurements in 2A panel were done at 12 μM per subunit total protein concentration. All holoHb unfolding measurements were done in 200 mM potassium phosphate (pH 7) at 10 °C. Protein samples were initially prepared in aqua-met oxidation states.

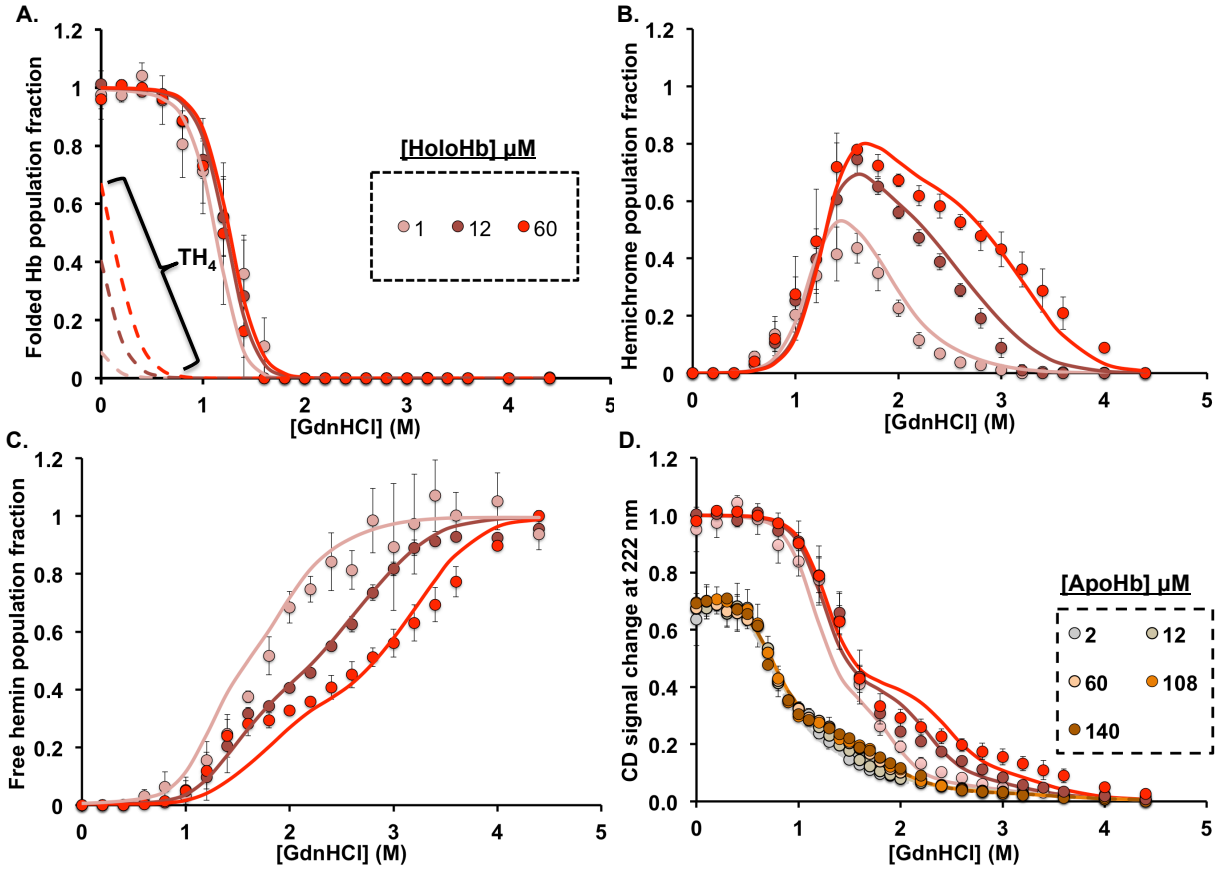

Figure 3. **Fittings of holoHbA GdnHCl-induced disassembly measurements to HbA equilibrium disassembly model 1**. The solid circles are the measured data at different per subunit total protein concentration, the solid lines are the fits, and the dashed lines are the theoretical population fraction of folded holoHbA tetramers (TH_4) derived from the fittings. A. Population fractions of aquamet- holoHb dimers and tetramers. B. Population fractions of hemichromes. C. Population fractions of free hemin. D. Fractional CD change at 222 nm, a measure in the change of alpha-helical structure content relative to folded holoHbA. The apoHbA unfolding measurements (curves at the far left) were obtained from previously published data[4]. The experimental measurements in A-C panels were obtained from deconvolution of visible absorbance spectra recorded between 350 nm and 660 nm. All holoHb unfolding measurements were done in 200 mM potassium phosphate (pH 7) at 10 °C. Protein samples were initially prepared in aqua-met oxidation states. Each data point is an average of triplicate titrations of protein with denaturant.

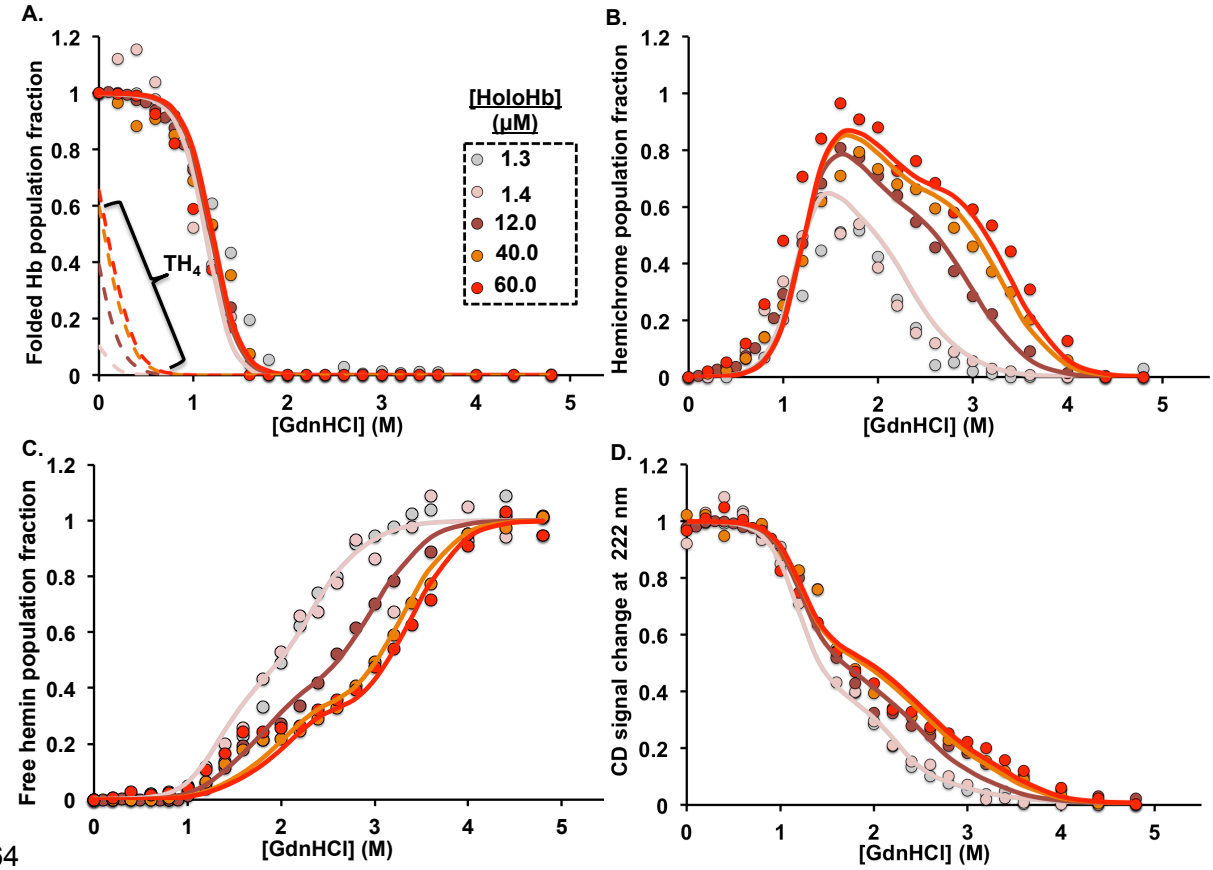

Figure 4. **Fittings of holoHbF GdnHCl-induced disassembly measurements to HbA equilibrium disassembly model 1**. The solid circles are the measured data at different per subunit total protein concentration, solid lines are the fits, and dashed lines are the theoretical population fraction of folded holoHbF tetramers (TH_4) derived from the fittings. A. Population fractions of aquamet- holoHb dimers and tetramers. B. Population fractions of hemichromes. C. Population fractions of free hemin. D. Fractional CD change at 222 nm, a measure in the change of alpha-helical structure content relative to folded holoHbF. The experimental measurements in A-C panels were obtained from deconvolution of visible absorbance spectra recorded between 350 nm and 660 nm. All holoHb unfolding measurements were done in 200 mM potassium phosphate (pH 7) at 10 °C. Protein samples were initially prepared in aqua-met oxidation states. The 12 μM Hb CD unfolding measurement was obtained from previously published data [4].

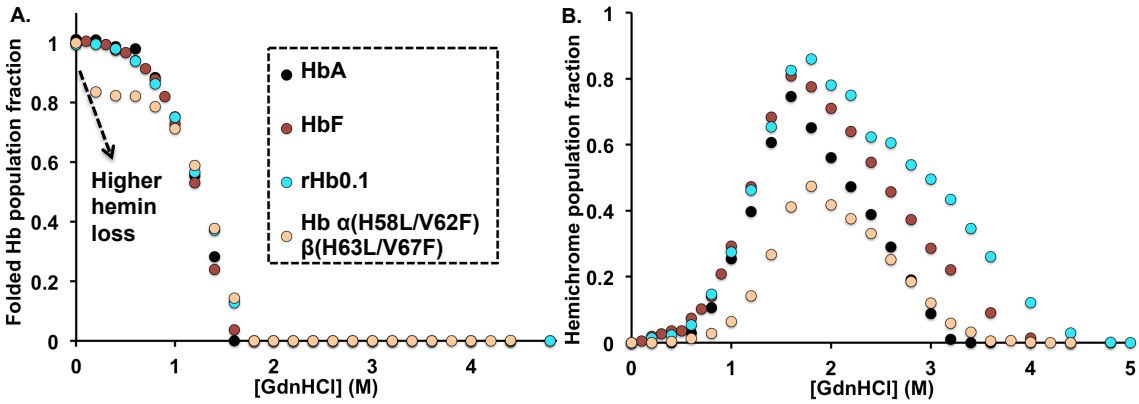

Figure 5. **Comparison of GdnHCl-induced equilibrium unfolding measurements of holo-HbA, HbF, rHb0.1, and Hb α(H58L/V62F)β(H63L/V67F).** The solid circles are the measured data at 12 μM per subunit total protein concentration. A. Population fractions of met- holoHb dimers and tetramers. B. Population fractions of hemichromes. The experimental measurements were obtained from deconvolution of visible absorbance spectra recorded between 350 nm and 660 nm. All holoHb unfolding measurements were done in 200 mM potassium phosphate (pH 7) at 10 °C. Protein samples were initially prepared in met oxidation states.

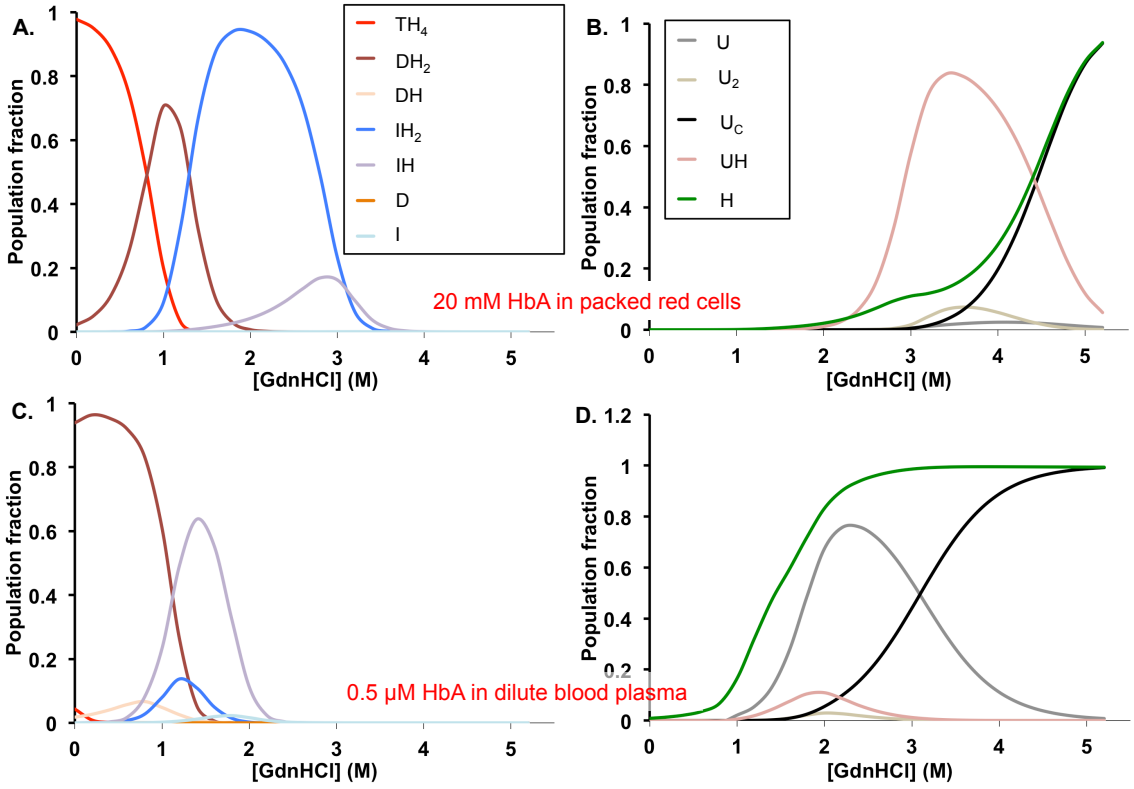

Figure 6. **Simulated HbA disassembly population fractions** in A. **Hb packed red blood cells and** B. **dilute blood plasma** demonstrate Hb concentration directed disassembly pathways. Simulations were done using Model 1 (Figure 1) and the parameters in Table1 as a factor of GdnHCl.

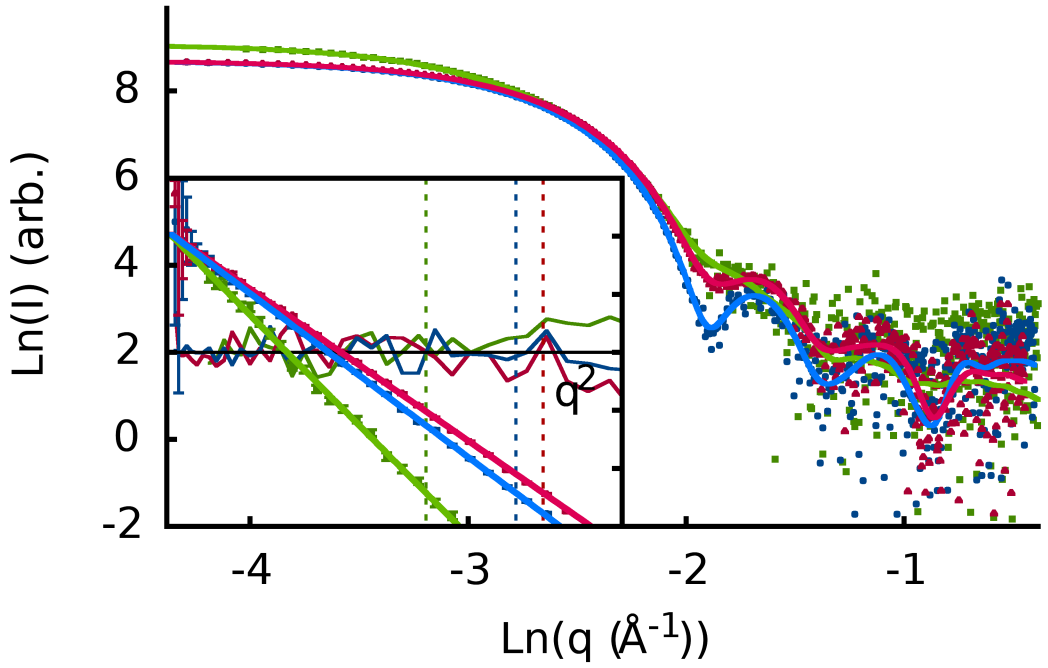

Figure 7. **SAXS Log intensity profiles and Guiner plot (inset) for recombinant hemoglobins.** For the Log-Log plots, the samples shown are the zero-concentration extrapolated aporHb0.0 (green), 2.0 mg/ml Hb0.1 (blue) and 2.0 mg/ml Hb0.0 (red) Inset: The Guinier plots with their residuals (darker lines) and ($1.3/R_g$) Guinier q-upper limits (dashed lines for R_g=29.4, 24.3, 23.6 Å). The expansion of the apoprotein is obvious from the less distinct minima in the higher angle data.

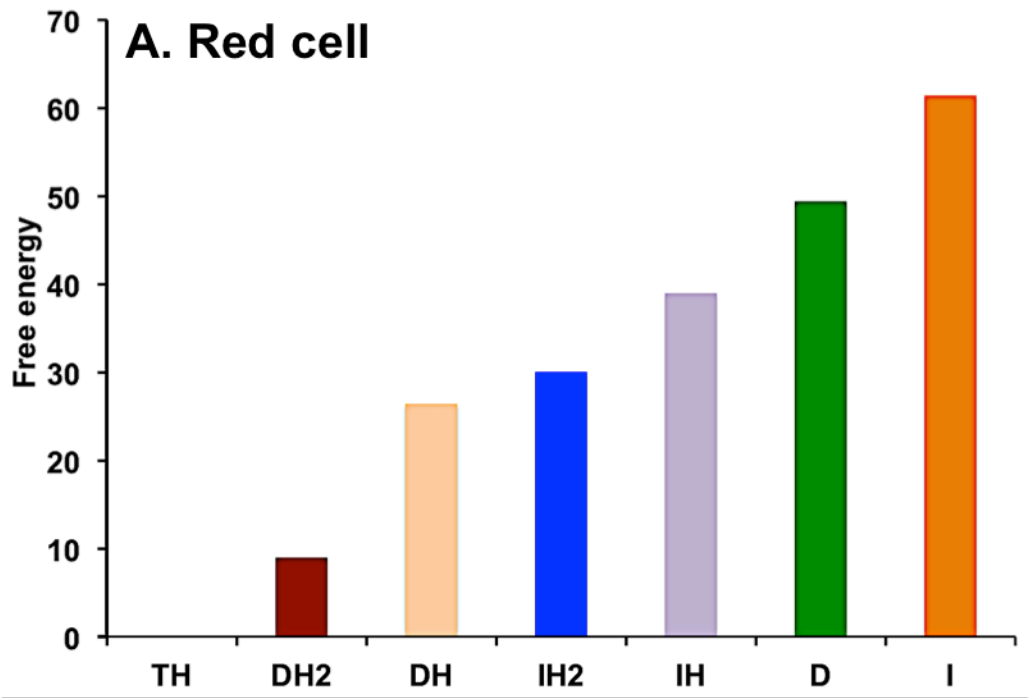

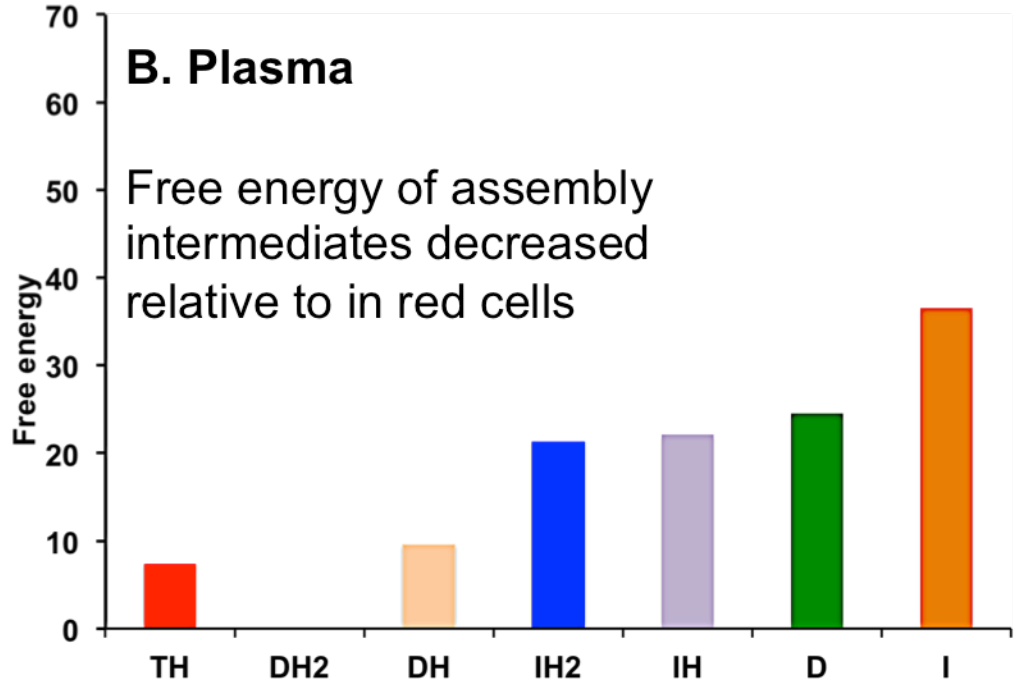

Figure 8. **Predicted relative free energies of various Hb disassembly intermediates** in A. red cells and B. diluted into plasma**.**

References

1. Schechter AN: **Hemoglobin research and the origins of molecular medicine**. *Blood* 2008, **112**(10):3927-3938.
2. Perutz MF: **Stereochemistry of cooperative effects in haemoglobin**. *Nature* 1970, **228**(5273):726-739.
3. Perutz MF: **Hemoglobin structure and respiratory transport**. *Scientific American* 1978, **239**(6):92-125.
4. Samuel PP, Ou WC, Phillips GN, Jr., Olson JS: **Mechanism of human apohemoglobin unfolding**. *Biochemistry* 2017, **56**(10):1444-1459.
5. Daniels KG, Tonthat NK, McClure DR, Chang YC, Liu X, Schumacher MA, Fierke CA, Schmidler SC, Oas TG: **Ligand concentration regulates the pathways of coupled protein folding and binding**. *Journal of the American Chemical Society* 2014, **136**(3):822-825.
6. Krantz BA, Sosnick TR: **Engineered metal binding sites map the heterogeneous folding landscape of a coiled coil**. *Nature structural biology* 2001, **8**(12):1042-1047.
7. Marsh JA, Teichmann SA: **Structure, dynamics, assembly, and evolution of protein complexes**. *Annual review of biochemistry* 2015, **84**:551-575.
8. Moran LB, Schneider JP, Kentsis A, Reddy GA, Sosnick TR: **Transition state heterogeneity in GCN4 coiled coil folding studied by using multisite mutations and crosslinking**. *Proceedings of the National Academy of Sciences of the United States of America* 1999, **96**(19):10699-10704.
9. Hargrove MS, Olson JS: **The stability of holomyoglobin is determined by heme affinity**. *Biochemistry* 1996, **35**(35):11310-11318.
10. Scott EE, Paster EV, Olson JS: **The stabilities of mammalian apomyoglobins vary over a 600-fold range and can be enhanced by comparative mutagenesis**. *The Journal of biological chemistry* 2000, **275**(35):27129-27136.
11. Culbertson DS, Olson JS: **Role of heme in the unfolding and assembly of myoglobin**. *Biochemistry* 2010, **49**(29):6052-6063.
12. Waugh SM, Low PS: **Hemichrome binding to band 3: nucleation of Heinz bodies on the erythrocyte membrane**. *Biochemistry* 1985, **24**(1):34-39.
13. Aessopos A, Kati M, Farmakis D: **Heart disease in thalassemia intermedia: a review of the underlying pathophysiology**. *Haematologica* 2007, **92**(5):658-665.
14. Aessopos A, Farmakis D, Deftereos S, Tsironi M, Tassiopoulos S, Moyssakis I, Karagiorga M: **Thalassemia heart disease: a comparative evaluation of thalassemia major and thalassemia intermedia**. *Chest* 2005, **127**(5):1523-1530.
15. Umbreit J: **Methemoglobin--it's not just blue: a concise review**. *American journal of hematology* 2007, **82**(2):134-144.
16. Peisach J, Blumberg WE, Rachmilewitz EA: **The demonstration of ferrihemochrome intermediates in heinz body formation following the reduction of oxyhemoglobin A by acetylphenylhydrazone**. *Biochimica et biophysica acta* 1975, **393**(2):404-418.
17. Winterbourn CC, Carrell RW: **Studies of hemoglobin denaturation and Heinz body formation in the unstable hemoglobins**. *The Journal of clinical investigation* 1974, **54**(3):678-689.
18. Winterbourn CC, Carrell RW: **Characterization of Heinz bodies in unstable haemoglobin haemolytic anaemia**. *Nature* 1972, **240**(5377):150-152.
19. Williamson D: **The unstable haemoglobins**. *Blood reviews* 1993, **7**(3):146-163.
20. Forget BG, Bunn HF: **Classification of the disorders of hemoglobin**. *Cold Spring Harbor perspectives in medicine* 2013, **3**(2):a011684.
21. Antonini E, Brunori M: **Hemoglobin and myoglobin in their reactions with ligands**: North-Holland Pub. Co.; 1971.
22. Hargrove MS, Whitaker T, Olson JS, Vali RJ, Mathews AJ: **Quaternary structure regulates hemin dissociation from human hemoglobin**. *The Journal of biological chemistry* 1997, **272**(28):17385-17389.

23. Zhang L, Levy A, Rifkind JM: **Autoxidation of hemoglobin enhanced by dissociation into dimers**. *The Journal of biological chemistry* 1991, **266**(36):24698-24701.
24. Mollan TL, Jia Y, Banerjee S, Wu G, Kreulen RT, Tsai AL, Olson JS, Crumbliss AL, Alayash AI: **Redox properties of human hemoglobin in complex with fractionated dimeric and polymeric human haptoglobin**. *Free Radical Biology & Medicine* 2014, **69**:265-277.
25. Brantley RE, Jr., Smerdon SJ, Wilkinson AJ, Singleton EW, Olson JS: **The mechanism of autooxidation of myoglobin**. *The Journal of biological chemistry* 1993, **268**(10):6995-7010.
26. Rifkind JM, Abugo O, Levy A, Heim J: **Detection, formation, and relevance of hemichromes and hemochromes**. *Methods in Enzymology* 1994, **231**:449-480.
27. Harrington JP, Newton P, Crumpton T, Keaton L: **Induced hemichrome formation of methemoglobins A, S and F by fatty acids, alkyl ureas and urea**. *The International journal of biochemistry* 1993, **25**(5):665-670.
28. Ogunmola GB, Zipp A, Chen F, Kauzmann W: **Effects of pressure on visible spectra of complexes of myoglobin, hemoglobin, cytochrome c, and horse radish peroxidase**. *Proceedings of the National Academy of Sciences of the United States of America* 1977, **74**(1):1-4.
29. Rachmilewitz EA: **Formation of hemichromes from oxidized hemoglobin subunits**. *Annals of the New York Academy of Sciences* 1969, **165**(1):171-184.
30. Fotouhi L, Yousefinejad S, Salehi N, Saboury AA, Sheibani N, Moosavi-Movahedi AA: **Application of merged spectroscopic data combined with chemometric analysis for resolution of hemoglobin intermediates during chemical unfolding**. *Spectrochimica acta Part A, Molecular and biomolecular spectroscopy* 2015, **136 Pt C**:1974-1981.
31. Bunn HF, Forget BG: **Hemoglobin Structure**. In: *Hemoglobin--molecular, genetic, and clinical aspects.* Philadelphia: W.B. Saunders Co.; 1986: 13-35.
32. Frier JA, Perutz MF: **Structure of human foetal deoxyhaemoglobin**. *Journal of molecular biology* 1977, **112**(1):97-112.
33. Rachmilewitz EA, Peisach J, Blumberg WE: **Studies on the stability of oxyhemoglobin A and its constituent chains and their derivatives**. *The Journal of biological chemistry* 1971, **246**(10):3356-3366.
34. Eliezer D, Wright PE: **Is apomyoglobin a molten globule? Structural characterization by NMR**. *Journal of molecular biology* 1996, **263**(4):531-538.
35. Yip YK, Waks M, Beychok S: **Influence of prosthetic groups on protein folding and subunit assembly. I. Conformational differences between separated human alpha- and beta-globins**. *The Journal of biological chemistry* 1972, **247**(22):7237-7244.
36. Fanelli AR, Antonini E, Caputo A: **Studies on the structure of hemoglobin. I. Physicochemical properties of human globin**. *Biochimica et biophysica acta* 1958, **30**(3):608-615.
37. Winterhalter KH, Huehns ER: **Preparations, properties, and specific recombination of alpha-beta-globin subunits**. *The Journal of biological chemistry* 1964, **239**:3699-3705.
38. Benesch RE, Kwong S: **The stability of the heme-globin linkage in some normal, mutant, and chemically modified hemoglobins**. *The Journal of biological chemistry* 1990, **265**(25):14881-14885.
39. Cassoly R, Bucci E, Iwatsubo M, Banerjee R: **Functional studies on human semi-hemoglobin**. *Biochimica et biophysica acta* 1967, **133**(3):557-567.
40. Bunn HF, Jandl JH: **Exchange of heme among hemoglobins and between hemoglobin and albumin**. *The Journal of biological chemistry* 1968, **243**(3):465-475.
41. Vasudevan G, McDonald MJ: **Spectral demonstration of semihemoglobin formation during CN-hemin incorporation into human apohemoglobins**. *The Journal of biological chemistry* 1997, **272**(1):517-524.
42. Robinson CR, Liu Y, Thomson JA, Sturtevant JM, Sligar SG: **Energetics of heme binding to native and denatured states of cytochrome b562**. *Biochemistry* 1997, **36**(51):16141-16146.
43. Landfried DA, Vuletich DA, Pond MP, Lecomte JT: **Structural and thermodynamic consequences of b heme binding for monomeric apoglobins and other apoproteins**. *Gene* 2007, **398**(1-2):12-28.

1130 44. Samuel PP, Smith LP, Phillips GN, Jr., Olson JS: **Apoglobin stability is the major factor**
1131 **governing both cell-free and *in vivo* expression of holomyoglobin**. *The Journal of biological*
1132 *chemistry* 2015, **290**(39):23479-23495.
1133 45. Berzofsky JA, Peisach J, Horecker BL: **Sulfheme proteins. IV. The stoichiometry of sulfur**
1134 **incorporation and the isolation of sulfhemin, the prosthetic group of sulfmyoglobin**. *The*
1135 *Journal of biological chemistry* 1972, **247**(12):3783-3791.
1136 46. de Villiers KA, Kaschula CH, Egan TJ, Marques HM: **Speciation and structure of**
1137 **ferriprotoporphyrin IX in aqueous solution: spectroscopic and diffusion measurements**
1138 **demonstrate dimerization, but not mu-oxo dimer formation**. *J Biol Inorg Chem* 2007,
1139 **12**(1):101-117.
1140 47. Culbertson DS: **Role of heme in the folding and assembly of globins**. *Doctoral Thesis.*
1141 Houston, Texas: Rice University; 2011.
1142 48. Vergara A, Vitagliano L, Verde C, di Prisco G, Mazzarella L: **Spectroscopic and**
1143 **crystallographic characterization of bis-histidyl adducts in tetrameric hemoglobins**.
1144 *Methods in Enzymology* 2008, **436**:425-444.
1145 49. Hensley P, Edelstein SJ, Wharton DC, Gibson QH: **Conformation and spin state in**
1146 **methemoglobin**. *The Journal of biological chemistry* 1975, **250**(3):952-960.
1147 50. Yi J, Thomas LM, Richter-Addo GB: **Structure of human R-state aquomethemoglobin at 2.0**
1148 **A resolution**. *Acta crystallographica Section F, Structural biology and crystallization*
1149 *communications* 2011, **67**(Pt 6):647-651.
1150 51. Bisse E, Schaeffer-Reiss C, Van Dorsselaer A, Alayi TD, Epting T, Winkler K, Benitez Cardenas
1151 AS, Soman J, Birukou I, Samuel PP *et al*: **Hemoglobin Kirklareli (alpha H58L), a new variant**
1152 **associated with iron deficiency and increased CO binding**. *The Journal of biological*
1153 *chemistry* 2017, **292**(6):2542-2555.
1154 52. Hargrove MS, Wilkinson AJ, Olson JS: **Structural factors governing hemin dissociation**
1155 **from metmyoglobin**. *Biochemistry* 1996, **35**(35):11300-11309.
1156 53. Gilat A, Subraniam V: **Solving Nonlinear Equations**. In: *Numerical methods for engineers and*
1157 *scientists.* Hoboken, New Jersey: John Wiley & Sons, Inc; 2011: 81-87.
1158 54. Strader MB, Bangle R, Parker Siburt CJ, Varnado CL, Soman J, Benitez Cardenas AS, Samuel
1159 PP, Singleton EW, Crumbliss AL, Olson JS *et al*: **Engineering oxidative stability in human**
1160 **hemoglobin based on the Hb providence (betaK82D) mutation and genetic cross-linking**.
1161 *The Biochemical journal* 2017, **474**(24):4171-4192.
1162 55. Adair GS: **The hemoglobin system. VI. The oxygen dissociation curve of hemoglobin**. *J*
1163 *Biol Chem* 1925, **63**(2):529-545.
1164 56. Moras M, Lefevre SD, Ostuni MA: **From Erythroblasts to Mature Red Blood Cells: Organelle**
1165 **Clearance in Mammals**. *Frontiers in physiology* 2017, **8**:1076.
1166 57. Coin JT, Olson JS: **The rate of oxygen uptake by human red blood cells**. *The Journal of*
1167 *biological chemistry* 1979, **254**(4):1178-1190.
1168 58. Ney PA: **Normal and disordered reticulocyte maturation**. *Current opinion in hematology*
1169 2011, **18**(3):152-157.
1170 59. Chu AH, Ackers GK: **Mutual effects of protons, NaCl, and oxygen on the dimer-tetramer**
1171 **assembly of human hemoglobin. The dimer Bohr effect**. *The Journal of biological chemistry*
1172 1981, **256**(3):1199-1205.
1173 60. Manning LR, Jenkins WT, Hess JR, Vandegriff K, Winslow RM, Manning JM: **Subunit**
1174 **dissociations in natural and recombinant hemoglobins**. *Protein science : a publication of*
1175 *the Protein Society* 1996, **5**(4):775-781.
1176 61. Vinchi F, Tolosano E: **Therapeutic approaches to limit hemolysis-driven endothelial**
1177 **dysfunction: scavenging free heme to preserve vasculature homeostasis**. *Oxidative*
1178 *medicine and cellular longevity* 2013, **2013**:396527.
1179 62. Schaer DJ, Buehler PW: **Cell-free hemoglobin and its scavenger proteins: new disease**
1180 **models leading the way to targeted therapies**. *Cold Spring Harbor perspectives in medicine*
1181 2013, **3**(6).

1182 63. Schaer DJ, Buehler PW, Alayash AI, Belcher JD, Vercellotti GM: **Hemolysis and free**
1183 **hemoglobin revisited: exploring hemoglobin and hemin scavengers as a novel class of**
1184 **therapeutic proteins**. *Blood* 2013, **121**(8):1276-1284.
1185 64. Fairbanks VF, Ziesmer SC, O'Brien PC: **Methods for measuring plasma hemoglobin in**
1186 **micromolar concentration compared**. *Clinical chemistry* 1992, **38**(1):132-140.
1187 65. Adamzik M, Hamburger T, Petrat F, Peters J, de Groot H, Hartmann M: **Free hemoglobin**
1188 **concentration in severe sepsis: methods of measurement and prediction of outcome**.
1189 *Critical care* 2012, **16**(4):R125.
1190 66. Quaye IK: **Extracellular hemoglobin: the case of a friend turned foe**. *Frontiers in physiology*
1191 2015, **6**:96.
1192 67. Looker D, Abbott-Brown D, Cozart P, Durfee S, Hoffman S, Mathews AJ, Miller-Roehrich J,
1193 Shoemaker S, Trimble S, Fermi G *et al*: **A human recombinant haemoglobin designed for**
1194 **use as a blood substitute**. *Nature* 1992, **356**(6366):258-260.
1195 68. Looker D, Mathews AJ, Neway JO, Stetler GL: **Expression of recombinant human**
1196 **hemoglobin in Escherichia coli**. *Methods in Enzymology* 1994, **231**:364-374.
1197 69. Hoffman SJ, Looker DL, Roehrich JM, Cozart PE, Durfee SL, Tedesco JL, Stetler GL:
1198 **Expression of fully functional tetrameric human hemoglobin in Escherichia coli**.
1199 *Proceedings of the National Academy of Sciences of the United States of America* 1990,
1200 **87**(21):8521-8525.
1201 70. Kikhney AG, Svergun DI: **A practical guide to small angle X-ray scattering (SAXS) of**
1202 **flexible and intrinsically disordered proteins**. *FEBS letters* 2015, **589**(19 Pt A):2570-2577.
1203 71. Burmester T, Ebner B, Weich B, Hankeln T: **Cytoglobin: a novel globin type ubiquitously**
1204 **expressed in vertebrate tissues**. *Molecular biology and evolution* 2002, **19**(4):416-421.
1205 72. Ptitsyn OB, Ting KL: **Non-functional conserved residues in globins and their possible role**
1206 **as a folding nucleus**. *Journal of molecular biology* 1999, **291**(3):671-682.
1207 73. Olsen KW: **Thermal denaturation procedures for hemoglobin**. *Methods in Enzymology* 1994,
1208 **231**:514-524.
1209 74. Yan YB, Wang Q, He HW, Zhou HM: **Protein thermal aggregation involves distinct regions:**
1210 **sequential events in the heat-induced unfolding and aggregation of hemoglobin**.
1211 *Biophysical journal* 2004, **86**(3):1682-1690.
1212 75. Michnik A, Drzazga Z, Kluczewska A, Michalik K: **Differential scanning microcalorimetry**
1213 **study of the thermal denaturation of haemoglobin**. *Biophysical chemistry* 2005, **118**(2-3):93-
1214 101.
1215 76. Hargrove MS, Barrick D, Olson JS: **The association rate constant for heme binding to**
1216 **globin is independent of protein structure**. *Biochemistry* 1996, **35**(35):11293-11299.
1217 77. Hebbel RP, Morgan WT, Eaton JW, Hedlund BE: **Accelerated autoxidation and heme loss**
1218 **due to instability of sickle hemoglobin**. *Proceedings of the National Academy of Sciences of*
1219 *the United States of America* 1988, **85**(1):237-241.
1220 78. Komar AA, Kommer A, Krasheninnikov IA, Spirin AS: **Cotranslational heme binding to**
1221 **nascent globin chains**. *FEBS letters* 1993, **326**(1-3):261-263.
1222 79. Khan AA, Quigley JG: **Control of intracellular heme levels: heme transporters and heme**
1223 **oxygenases**. *Biochimica et biophysica acta* 2011, **1813**(5):668-682.
1224 80. Davis CM, Gruebele M, Sukenik S: **How does solvation in the cell affect protein folding and**
1225 **binding?** *Current opinion in structural biology* 2018, **48**:23-29.
1226 81. Mu X, Choi S, Lang L, Mowray D, Dokholyan NV, Danielsson J, Oliveberg M: **Physicochemical**
1227 **code for quinary protein interactions in Escherichia coli**. *Proceedings of the National*
1228 *Academy of Sciences of the United States of America* 2017, **114**(23):E4556-E4563.
1229 82. Belcher JD, Beckman JD, Balla G, Balla J, Vercellotti G: **Heme degradation and vascular**
1230 **injury**. *Antioxidants & redox signaling* 2010, **12**(2):233-248.
1231 83. Cardenas ASB, Samuel PP, Olson JS: **2017 Military Supplement: Current Challenges in the**
1232 **Development of Acellular Hemoglobin Oxygen Carriers by Protein Engineering**. *Shock*
1233 2017.
1234 84. Faivre B, Menu P, Labrude P, Vigneron C: **Hemoglobin autooxidation/oxidation**
1235 **mechanisms and methemoglobin prevention or reduction processes in the bloodstream.**

Literature review and outline of autooxidation reaction. *Artificial cells, blood substitutes, and immobilization biotechnology* 1998, **26**(1):17-26.

85. Kosaka H, Uozumi M, Tyuma I: **The interaction between nitrogen oxides and hemoglobin and endothelium-derived relaxing factor**. *Free Radical Biology & Medicine* 1989, **7**(6):653-658.
86. Young JD, Dyar O, Xiong L, Howell S: **Methaemoglobin production in normal adults inhaling low concentrations of nitric oxide**. *Intensive care medicine* 1994, **20**(8):581-584.
87. Larsen R, Gouveia Z, Soares MP, Gozzelino R: **Heme cytotoxicity and the pathogenesis of immune-mediated inflammatory diseases**. *Frontiers in pharmacology* 2012, **3**:77.
88. Baek JH, D'Agnillo F, Vallelian F, Pereira CP, Williams MC, Jia Y, Schaer DJ, Buehler PW: **Hemoglobin-driven pathophysiology is an in vivo consequence of the red blood cell storage lesion that can be attenuated in guinea pigs by haptoglobin therapy**. *The Journal of clinical investigation* 2012, **122**(4):1444-1458.
89. Kumar S, Bandyopadhyay U: **Free heme toxicity and its detoxification systems in human**. *Toxicology letters* 2005, **157**(3):175-188.
90. Belcher JD, Nath KA, Vercellotti GM: **Vasculotoxic and Proinflammatory Effects of Plasma Heme: Cell Signaling and Cytoprotective Responses**. *ISRN oxidative medicine* 2013, **2013**.
91. Figueiredo RT, Fernandez PL, Mourao-Sa DS, Porto BN, Dutra FF, Alves LS, Oliveira MF, Oliveira PL, Graca-Souza AV, Bozza MT: **Characterization of heme as activator of Toll-like receptor 4**. *The Journal of biological chemistry* 2007, **282**(28):20221-20229.
92. Shen TJ, Ho NT, Simplaceanu V, Zou M, Green BN, Tam MF, Ho C: **Production of unmodified human adult hemoglobin in Escherichia coli**. *Proceedings of the National Academy of Sciences of the United States of America* 1993, **90**(17):8108-8112.
93. Shen TJ, Ho NT, Zou M, Sun DP, Cottam PF, Simplaceanu V, Tam MF, Bell DA, Jr., Ho C: **Production of human normal adult and fetal hemoglobins in Escherichia coli**. *Protein engineering* 1997, **10**(9):1085-1097.
94. Maillett DH: **Engineering hemoglobins and myoglobins for efficient oxygen transport**. *Doctoral* Houston, Texas: Rice University; July, 2003.
95. Elmer J, Harris D, Palmer AF: **Purification of hemoglobin from red blood cells using tangential flow filtration and Immobilized metal ion affinity chromatography**. *J Chromatogr B Analyt Technol Biomed Life Sci* 2011, **879**(2):131-138.
96. Shelton JB, Shelton JR, Schroeder WA: **High Performance Liquid Chromatographic Separation of Globin Chains on a Large-Pore C4 Column**. *Journal of Liquid Chromatography* 1984, **7**(10):1969-1977.
97. Samuel PP: **Expression, Folding, and Assembly Mechanisms of Monomeric Myoglobins and Oligomeric Hemoglobins**. Houston, TX: Rice University; 2017.
98. Birukou I, Schweers RL, Olson JS: **Distal histidine stabilizes bound O2 and acts as a gate for ligand entry in both subunits of adult human hemoglobin**. *The Journal of biological chemistry* 2010, **285**(12):8840-8854.
99. Hargrove MS, Singleton EW, Quillin ML, Ortiz LA, Phillips GN, Jr., Olson JS, Mathews AJ: **His64(E7)-->Tyr apomyoglobin as a reagent for measuring rates of hemin dissociation**. *The Journal of biological chemistry* 1994, **269**(6):4207-4214.
100. Ascoli F, Fanelli MR, Antonini E: **Preparation and properties of apohemoglobin and reconstituted hemoglobins**. *Methods in Enzymology* 1981, **76**:72-87.
101. Kumar Sau A, Currell D, Mazumdar S, Mitra S: **Interaction of sodium dodecyl sulfate with human native and cross-linked hemoglobins: a transient kinetic study**. *Biophysical chemistry* 2002, **98**(3):267-273.
102. Quillin ML, Arduini RM, Olson JS, Phillips GN, Jr.: **High-resolution crystal structures of distal histidine mutants of sperm whale myoglobin**. *Journal of molecular biology* 1993, **234**(1):140-155.
103. Grishaev A: **Sample preparation, data collection, and preliminary data analysis in biomolecular solution X-ray scattering**. *Current protocols in protein science* 2012, **Chapter 17**:Unit17 14.

1289 104. Putnam CD, Hammel M, Hura GL, Tainer JA: **X-ray solution scattering (SAXS) combined**
1290 **with crystallography and computation: defining accurate macromolecular structures,**
1291 **conformations and assemblies in solution**. *Quarterly reviews of biophysics* 2007, **40**(3):191-
1292 285.
1293 105. Franke D, Petoukhov MV, Konarev PV, Panjkovich A, Tuukkanen A, Mertens HDT, Kikhney AG,
1294 Hajizadeh NR, Franklin JM, Jeffries CM *et al*: **ATSAS 2.8: a comprehensive data analysis**
1295 **suite for small-angle scattering from macromolecular solutions**. *Journal of applied*
1296 *crystallography* 2017, **50**(Pt 4):1212-1225.
1297